Time domain imaging of transient and variable radio sources

Cendes, Y.N.

Hoofdstuk 4

A Time-Domain Survey of Luminous Local Radio Sources on 25 Year Timescales

Yvette Cendes, Bryan Gaensler, Casey Law

to be submitted

Abstract

We consider 117 extragalactic radio sources as potential transient and variable sources that were listed in a catalog of luminous local (<108 Mpc) radio sources as possible persistent Fast Radio Burst (FRB) counterparts. We used observations from the Very Large Array Sky Survey (VLASS) at 3 GHz and the Faint Images of the Radio Sky at Twenty-cm (FIRST) catalog at 1.4 GHz ∼25 years earlier in order to establish changes in flux over time in our sample, and compiled detailed light curves using data from multiple radio surveys for 19 of these sources. We also included X-ray observations of these sources, both from the ROSAT catalog and from analysis of available Swift XRT images, but our X-ray analysis yielded non-detections. We identified one transient candidate, FIRST J235351.4+075835, which has faded monotonically by a factor of ∼ 2 over 20 years, which may be due to a tidal disruption event (TDE) or neutron star merger. However, this source lacks an optical counterpart, so a definitive conclusion on the nature of the source would require additional optical follow-up observations. We conclude the rest of our sources which display variable behavior are likely caused by low excitation radio galaxies (LERG) with emission caused by low, inefficient accretion onto a supermassive black hole.

4.1 Introduction

Thanks to rapidly advancing detector technology and faster computing speeds, in recent years the discovery of radio transients on short time scales (seconds to months) has become increasingly common. However, considerably less effort has been devoted to finding transients on the longer time scales that last from years to decades. In particular, the lack of extensive sub-mJy data over a significant fraction of sky before large surveys such as the NRAO-VLA Sky Survey [NVSS; Condon et al., 1998] and the Westerbork Northern Sky Survey [WENSS; Rengelink et al., 1997] in the ∼1990s greatly limited the ability to find decades-long transients until sufficient time had passed.

Despite this limitation, the radio sky does have transient and variable sources on these timescales. Bannister et al. [2011] conducted a 22 year survey with the Molonglo Observatory Synthesis Telescope (MOST) at sub-mJy sensitivity at 843 MHz, and discovered several dozen transient and variable radio sources. The Stripe 82 survey [Mooley et al., 2016] using the Very Large Array (VLA) established that ∼3.9% of the thousands of radio sources observed at 3 GHz varied by >30% over a two year period. By comparing the TIFR GMRT Sky Survey Alternative Data Release 1 (TGSS ADR1) and the GaLactic and Extragalactic All-sky Murchison Widefield Array (GLEAM) survey catalogues, taken ∼3 years apart, Murphy et al. [2017] reported the discovery of one transient at these time scales. However, no comprehensive all-sky census on these timescales for transients exists because of the limitations of the data and the long time spans involved.

In the majority of the above cases, the transients and variables discovered are thought to be related to active galactic nucleus (AGN) activity [Bannister et al., 2011; Mooley et al., 2016]. Given that the majority of radio sources in the sky for which S > 1 mJy are AGN at 1.4 GHz [Becker et al., 1994], this is unsurprising. AGN variability on time scales of years to decades is common, and is likely to be due to relatively minor changes in the accretion flow onto a supermassive black hole that lead to a temporary change in luminosity of the non-thermal accretion disk emission [Tadhunter, 2016].

Within the population of AGN, quiescent, low-level AGN activity accounts for ∼60% of all AGN [Padovani et al., 2011], and they reach a peak luminosity in radio of $L_\nu = 10^{27} - 10^{34}$ erg s^{-1} Hz^{-1} at ∼1.5-5 GHz [Woo & Urry, 2002; Mooley et al., 2016]. Compared to this, more exotic long-term transients related to gamma-ray bursts (GRBs), tidal disruption events (TDEs), supernovae (SNe), and others are much more rare [Metzger et al., 2015; Mooley et al., 2016].

The recent discovery of FIRST J141918.9+394036 has provided an intriguing example of one such exotic long-term transient. FIRST J141918.9+394036 was a decades-long radio transient that faded by a factor of ∼50 over 23 years, and was no longer detectable by 2017 [Law et al., 2018]. It is thought the source is the afterglow of an off-axis ("orphan") long GRB.

FIRST J141918.9+394036 is also notable because it was discovered through a search relying on archival data from several previous surveys. First, the source was listed in a catalog of luminous ($L_\nu \leq 10^{28}$ erg s^{-1} Hz^{-1}) persistent radio sources in the nearby universe (defined as z ∼ 0.025, or < 108 Mpc), compiled from the Faint Images of the Radio Sky at Twenty-cm survey catalog [FIRST; Becker et al., 1994] and cross-matching with optical databases [Ofek, 2017]. The motivation behind the Ofek [2017] catalog was to identify nearby radio sources similar to the persistent radio counterpart of the first localized repeating Fast Radio Burst [FRB; Lorimer et al., 2007; Spitler

et al., 2016; Chatterjee et al., 2017], known as FRB 121102, and to establish the number density of bright compact persistent sources in the local universe. Ofek [2017] identified 122 possible candidates, of which 11 were identified as candidates associated with active star formation regions. Follow-up of these latter sources was conducted using available images from the Very Large Array Sky Survey (VLASS; Lacy et al. [2019]), which has recently observed the entire sky as seen from the VLA at 2-4 GHz. This in turn revealed the transient nature of FIRST J141918.9+394036.

Although Law et al. [2018] established that there is at least one interesting source within the Ofek [2017] catalog, the majority of sources from Ofek [2017] that were not associated with star forming regions were not examined in that work. Further, while Law et al. [2018] did measure the fluxes in VLASS for five of the other ten sources whose data was available at the time, the detailed light curves for these sources were not compiled. Here, we present the results of the remaining candidate radio signals in the Ofek [2017] catalog in the available VLASS images. From this analysis, we discuss the discovery of new luminous radio transients, and demonstrate what we can learn about variability in the local universe from studies that take advantage of several decades of existing archival data.

This chapter is divided as follows. In Section 4.2, we discuss the catalog of sources used in this study, their spectral indices, and the method used to identify variable sources. In Section 4.3, we discuss the 19 noteworthy sources identified through our study, including light curves that cover a range of ∼10-30 years, and discuss possible origins for all of them. In Section 4.4, we discuss these sources and how they are classified, including what they can tell us about the local variable radio population for luminous sources, the rate of variable luminous radio sources in this volume, and how our study compares to previous surveys. Finally, in Section 4.5, we discuss the conclusions from this work, and make recommendations for future searches.

4.2 Source Characterization

4.2.1 Catalog of Sources

The Ofek [2017] catalog of sources was compiled on the assumption that at least some FRBs will have luminous, persistent synchrotron radio counterparts similar to that seen for FRB 121102. As such, 122 potential FRB hosts were identified in or near nearby galaxies (< 108 Mpc, or $z < 0.025$) to place an upper limit on the number density of such sources in the local universe. Specifically, these sources had luminosities $> 10\%$ of the FRB 121102 persistent source luminosity, and had counterparts in FIRST, a project designed to produce the radio equivalent of the Palomar Observatory Sky Survey of the North and South Galactic Caps. Previous work by Law et al. [2018] focused on VLASS observations of the six candidates that overlapped with the optical light from a galactic disc or compact star forming galaxies which had been observed by VLASS at the time of publication, which were conditions similar to that found for FRB 121102 [Bassa et al., 2017]. The rest of the sources (85) that were within 1" of the center of the galaxy, and the 26 remaining sources not overlapping with light in a galactic disk, were not examined by Law et al. [2018].

To study these remaining sources, we used VLASS observations, which cover the entire sky as seen from the VLA at 2-4 GHz to 2.5" resolution. Our data included all the first VLASS epoch ("epoch 1"), which covered 100% of the observable sky from the VLA, although some

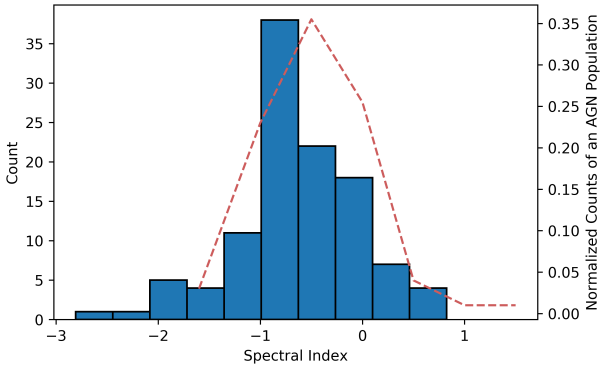

Figuur 4.1 The distribution of spectral indices for the sources in this work. We have overlaid the normalized counts for AGN from Zinn et al. [2012] for reference.

gaps exist due to calibration or noise issues. Epoch 1 is the first of three VLASS epochs, which will be separated by 36 months, with a sensitivity of 120 μJy/beam in a single epoch. Pipeline processed "quicklook" images are made available soon after observations take place, and we used these images to search for counterparts to the Ofek [2017] sources. We found that 117 individual sources were observed from the Ofek [2017] catalog, with two duplicate sources in the original catalog, and visual inspection of the VLASS images confirmed that three individual listings were, in fact, associated with a single extended source[1].

4.2.2 Source Association Between Surveys and Determination of Spectral indices

Our first step was to identify counterparts between the VLASS and FIRST images. As the typical positional error in FIRST images is $\leq$ 0.3"[White et al., 1997], and the VLASS positional error is $\sim$0.5"[Lacy et al., 2019], we defined the association radius between images as 1" in order to identify counterparts.

We obtained the VLASS quicklook images from the VLA archives that contained the sources in the Ofek [2017] catalog. We then used the source finding package Aegean [Hancock et al. (2018)] to create a file containing peak fluxes for all the sources in each VLASS image, and then

[1]The extended Source is located at 12:05:48.207, +20:27:48.27

checked for sources at the coordinates listed for our sources by Ofek [2017]. Once identified, we searched for catalog sources within our defined association radius of 1" from the VLASS sources, and found that all counterparts were within 1" of the source positions. All but three sources were detected to $\geq 3\sigma$ confidence. We discuss these sources in Section 4.3.

Next, we calculated a spectral index (α) for each source (rightmost column, Table 20), defined as:

$$\alpha = \frac{\log \frac{S_F}{S_V}}{\log \frac{\nu_F}{\nu_V}} \tag{4.1}$$

where S_F is the peak flux in FIRST, S_F is the peak flux in VLASS, ν_F is the mean frequency of FIRST (1.4 GHz), and ν_V is the frequency of VLASS (3 GHz). This was done because a spectral index calculation assumes the source has not varied, and thus an extreme or unusual index might be a sign of source variability. We calculated α based on the peak flux of the source in the FIRST catalog at 1.4 GHz, and our obtained VLASS peak source fluxes at 3 GHz.

The histogram distribution of these spectral indices can be seen in Figure 4.1. For the sources not detected in VLASS, we calculated the spectral index limit from the 3σ noise limit at the location of the coordinates, as measured in a forced fit using Aegean.

The coordinates for these sources, as well as their peak fluxes in FIRST, NVSS, VLASS and calculated spectral indices, are available in Table 20. A histogram of the spectral index distribution can be seen in Figure 4.1 as calculated from their peak fluxes in FIRST and VLASS. For reference, we have overlaid the distribution of spectral index for the population of AGN studied by Zinn et al. [2012], who calculated a 1.4 to 2.3 GHz spectral index for 120 AGN. We can see that our population as a whole has a steeper spectral index than the average. We also see there is an excess of sources for which $\alpha < -1.5$ in our source distribution when compared to that of the AGN population, and fewer positive sources than expected when compared to the Zinn et al. [2012] distribution.

4.2.3 Identifying Variability

As our primary interest lies in transient and radio sources, we adopted the variability statistic (V_s) defined by Mooley et al. [2016]. This is based on the flux densities of a source between two epochs and their respective errors:

$$V_s = \left| \frac{(S_1 - S_2)}{\sqrt{\sigma_1^2 + \sigma_2^2}} \right| = \left| \frac{\Delta S}{\sigma} \right| \geq 4.3 \tag{4.2}$$

Our threshold is V_s= 4.3 as defined by the t-statistic lying beyond the 95% confidence interval [see Equation 1 and associated footnote; Mooley et al., 2016].

Because FIRST and VLASS were at different frequencies (1.4 GHz and 3 GHz, respectively), we corrected the VLASS data in ΔS assuming a spectral index of -0.7, as an average value for α typical for nonthermal sources [de Gasperin et al., 2018]. We found that, once corrected, ten of our sources met our definition of variability, which we note in their relevant sections in Section 4.3.

For the ten individually identified sources, we compiled light curves spanning several decades based on existing data beyond what was included in Table 20. Additionally, we compiled light curves for seven sources identified as potential FRB counterparts by Ofek [2017], and two sources which displayed typical spectral indicies (α $\sim$-0.7) for illustrative purposes, for a total number of 19 sources studied in greater detail. The surveys we examined with data in the GHz regime were the high resolution imaging of survey data of Stripe 82 at 1.4 GHz [Hodge et al., 2011], and the Green Bank 4.85 GHz survey [GB6; Gregory et al., 1996]. At lower frequencies, we examined data from the VLA Low Frequency Sky Survey Redux [VLSSr; Peters et al., 2014] at 74 GHz, the 150 MHz TIFR GMRT Sky Survey (TGSS) survey using GMRT [Intema et al., 2017], the WENSS survey using the Westerbork Radio Telescope at 325 MHz [Rengelink et al., 1997], and the GaLactic and Extragalactic All-sky Murchison Widefield Array [GLEAM; Hurley-Walker et al., 2017] covering 72-231 MHz.

In addition to survey data, we examined the VLA archives and obtained several images that contained our sources of interest, stretching from 1984 to 2015. We include details of these images, where they exist, in their respective sections below.

For each of these data sets, we obtained the relevant radio images of the source, and used the sourcefinder Aegean to obtain the peak flux for the total intensity counterpart of the source at the FIRST coordinates. If the source was not detected with this method in the image, we performed a forced fit at the FIRST coordinates to obtain a 3σ upper limit on the radio source. We have starred each source in Table 20, and discuss our findings for each source below. We should also note that, for consistency in the light curve, we also re-measured the peak flux of our sources directly from FIRST images (as opposed to relying on the FIRST catalog values as we did in Section 4.2.2). In all cases, the fitted peak flux measured by the Aegean software was lower than the catalog value, and we include the updated spectral indices for these sources in their respective sections.

We also searched NASA's "GRB-CAT"compilation[2] and the 4Br BATSE gamma-ray burst catalog [Paciesas et al., 1999] for possible GRBs coincident with our radio sources. In all cases, all coincident GRBs had enormous (>20°) positional uncertainties, so we did not find these associations significant in relation to our sources.

We also examined the HEARC X-ray catalog for potential X-ray sources. We found that two sources had ROSAT catalog entries [Voges et al., 1999] coincident with the same location as the radio source. Additionally, we found six sources were coincident with archival Swift X-Ray Telescope [XRT; Burrows et al., 2005] observations, which we reduced and analyzed using standard practices. We discuss these X-ray findings in their relevant sections.

Additionally, we also did a visual inspection of all our sources using optical data from Sloan Digital Sky Survey [SDSS; York et al., 2000]. We include these in Section 4.3 where relevant.

4.3 Noteworthy Sources

The following are the sources that we looked at in greater detail. They are all sources considered interesting due to their variability statistics, as outlined in Section 4.2.3, or because they were

[2]See https://heasarc.gsfc.nasa.gov/grbcat/

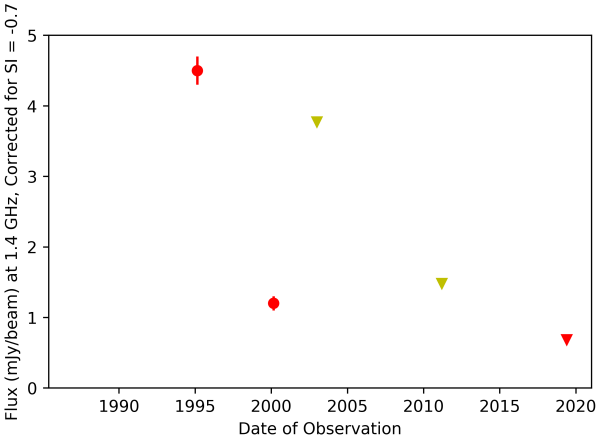

Figuur 4.2 Light curve over time for FIRST J143052.2+060209.6. Light curve for FIRST J143052.2+060209.6, corrected to 1.4 GHz for a spectral index of -0.7. We plot detections from 1.4 to 3 GHz in red, and 150 MHz in yellow, so as to distinguish between high and low frequency bands. Circular points signify detections of the source, and triangles are for the 3σ upper limits for non-detections. Here, we omit the data from Table 4.1 that are non-constraining.

one of the FRB-associated candidates noted by Ofek [2017].

4.3.1 Missing source: FIRST J143052.2+060209.6

FIRST J143052.2+060209.6 is notable in our survey because it was not detected in VLASS, for a 3σ upper limit of <0.4 mJy. This resulted in an implied spectral index of <-1.6. The source was detected by NVSS and FIRST, but was not detected by GB6, VLSSr, VLASS, or TGSS (Table 4.1). The light curve corrected for spectral index is visible in Figure 4.2, where we can see that it has decreased in brightness over time and has not been detected since 2000.

The host galaxy of the source is 2MASX J14305227+0602096, which is 113.2±7.9 Mpc distant [Hernández-Fernández et al., 2012]. This allows us to calculate a luminosity at peak flux in FIRST of $L = 6.9 \times 10^{28}$ erg s^{-1}Hz^{-1}. FIRST J143052.2+060209.6 is located at the center of its host galaxy.

Date of Observation	Peak Flux (mJy)	Observations	Frequency (GHz)
1987	<9	GB6	1.45
1995-02-27	4.5 ± 0.5	NVSS	1.4
2000-02-07	1.2 ± 0.2	FIRST	1.4
2003-09-20	<126	VLSSr	0.075
2011-02-11	<16	TGSS	0.15
2019-05-08	< 0.4	VLASS	2-4

Tabel 4.1 Table of flux values over time for FIRST J143052.2+060209.6. All non-detections are listed as 3σ upper limits.

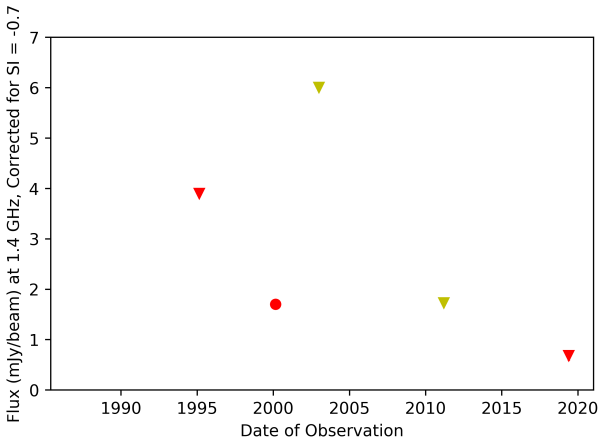

Figuur 4.3 As in Figure 4.2, but for FIRST J141430.5+060955.4.

4.3.2 Missing source: FIRST J141430.5+060955.4

FIRST J141430.5+060955.4 is notable in our survey because it was also not detected in VLASS, for a 3σ upper limit of <0.4 mJy. This resulted in an implied spectral index of <-1.9. The source was detected by FIRST, but was not detected by GB6, NVSS, VLSSr, or TGSS (Table 4.2). The light curve corrected for spectral index is visible in Figure 4.3, fitted to a spectral index of -1.2 because of the nearness in time of the high and low frequency FIRST and VLASS observations, respectively. We can see that this source was only detected once, when it was detected by FIRST as a 1.5 ± 0.1 mJy source.

The host galaxy of the source is LEDA 1295689, which is 92.8±6.5 Mpc distant [de Vaucouleurs et al., 1991]. This allows us to calculate a luminosity at peak flux from the FIRST observation of $L = 3.3 \times 10^{28}$ erg s^{-1}Hz^{-1}. FIRST J141430.5+060955.4 is located at the center of its host galaxy.

Date of Observation	Peak Flux (mJy)	Observations	Frequency (GHz)
1987	<18	GB6	4.85
1995-02-27	<3.9	NVSS	1.4
2000-02-01	1.7 ± 0.1	FIRST	1.4
2003-09-20	<245	VLSSr	0.075
2011-02-18	<20	TGSS	0.15
2019-05-08	<0.4	VLASS	2-4

Tabel 4.2 Table of flux values over time for FIRST J141430.5+060955.4. All non-detections are listed as 3σ upper limits.

4.3.3 FIRST J141043.6+085929

We examined FIRST J141043.6+085929 because it was noted as one of the 11 FRB-associated candidates by Ofek [2017]. The source was detected by NVSS, FIRST, and VLASS, but was

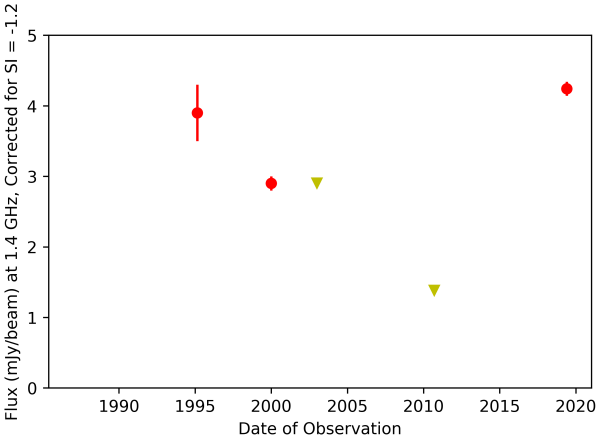

Figuur 4.4 As in Figure 4.2, but for FIRST J141043.6+085929.

not detected by GB6, VLSSr, or TGSS (Table 4.3). The light curve corrected for spectral index is visible in Figure 4.4. We can see that although it is brighter in VLASS than it was during its detection in FIRST, its non-detections by both VLSSr and TGSS indicate the source has fluctuated over time in flux.

The host galaxy of the source is CGCG 074-128, which is 107.3±7.5 Mpc distant [Beers et al., 1995]. This distance allows us to calculate a luminosity at peak flux from the FIRST observation of $L = 5.37 \times 10^{28}$ erg s^{-1}Hz^{-1}. FIRST J141043.6+085929 is located at the edge of a spiral galaxy, 17.7" from the center.

Additionally, we identified several Swift observations where the field of view included FIRST J235351.4+075835. However, none of these images had X-ray counts at its given location. The observation with the longest XRT exposure was observation 00010512023 taken on June 21, 2013, with 513 seconds of XRT exposure.

Date of Observation	Peak Flux (mJy)	Observations	Frequency (GHz)
1987	<80.7	GB6	4.85
1995-02-27	3.9 ± 0.4	NVSS	1.4
2000-01-02	2.9 ± 0.1	FIRST	1.4
2003-09-20	<46	VLSSr	0.075
2010-08-26	<12	TGSS	0.15
2019-05-08	1.7 ± 0.1	VLASS	2-4

Tabel 4.3 Table of flux values over time for FIRST J141043.6+085929. All non-detections are listed as 3σ upper limits.

4.3.4 FIRST J102526.1+171547

We examined FIRST J102526.1+171547 because it was noted as one of the 11 FRB-associated candidates by Ofek [2017]. The source was detected by NVSS, FIRST, and VLASS, but was not detected by GB6, VLSSr, TGSS, or a VLA observation from 1998 from the archives (Table

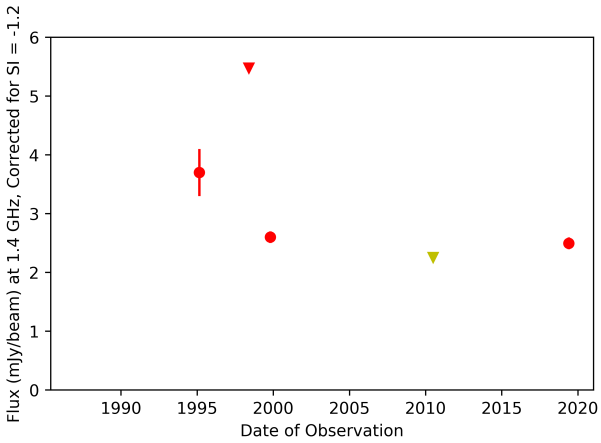

Figuur 4.5 As in Figure 4.2, but for FIRST J102526.1+171547.

4.4). The light curve corrected for spectral index is visible in Figure 4.5, where we can see it has remained relatively steady.

The host galaxy of the source is UGC 05639, which is 86.6±6.1 Mpc distant [Falco et al., 1999]. This distance allows us to calculate a luminosity at peak flux from the FIRST observation of $L = 2.3 \times 10^{28}$ erg s^{-1}Hz^{-1}. FIRST J102526.1+171547 is located in the spiral arm of a galaxy, 7.1" from the center.

Date of Observation	Peak Flux (mJy)	Observations	Frequency (GHz)
1987	<10.5	GB6	4.85
1993-12-06	3.7 ± 0.4	NVSS	1.4
1998-04-24	<5	VLA AM0236	1.51
1999-11-01	2.6 ± 0.1	FIRST	1.4
2003-09-20	<260	VLSSr	0.075
2010-06-15	<6	TGSS	0.15
2019-04-19	1.0 ± 0.1	VLASS	2-4

Tabel 4.4 Table of flux values over time for FIRST J141043.6+085929. All non-detections are listed as 3σ upper limits.

4.3.5 FIRST J105823.6+241355.3

We examined FIRST J105823.6+241355.3 because it was noted as one of the 11 FRB-associated candidates by Ofek [2017]. The source was by FIRST and VLASS, but was not detected by GB6, VLSSr or TGSS (Table 4.5). For the NVSS image, it was determined through the size of the beam fitted by the Aegean software and visual inspection of the NVSS image and comparison to the FIRST image that the NVSS source was unresolved, and in fact comprised of two sources. As such, we did not include this data in our analysis.

The light curve corrected for spectral index is visible in Figure 4.6. The source has decreased slightly in flux from its detections in FIRST to VLASS, assuming $\alpha = -0.7$.

Figuur 4.6 As in Figure 4.2, but for FIRST J105823.6+241355.3.

The host galaxy of the source is NGC 3475, which is 93.3±6.2 Mpc distant [de Vaucouleurs et al., 1991]. This distance allows us to calculate a luminosity at peak flux from the NVSS observation of $L = 2.1 \times 10^{28}$ erg s^{-1}Hz^{-1}. From our VLASS observation, where the source decreased in flux to of 0.7 ± 0.1 mJy, the source decreased to $L = 7.2 \times 10^{27}$ erg s^{-1}Hz^{-1} FIRST J105823.6+241355.3 is located in the spiral arm of a galaxy, 29.8" from the center.

Date of Observation	Peak Flux (mJy)	Observations	Frequency (GHz)
1987	<18	GB6	4.85
1995-12-08	2.1 ± 0.2	FIRST	1.4
2003-09-20	<123	VLSSr	0.075
2011-02-28	<76	TGSS	0.15
2019-06-08	0.7±0.1	VLASS	2-4

Tabel 4.5 Table of flux values over time for FIRST J105823.6+241355.3. All non-detections are listed as 3σ upper limits.

4.3.6 FIRST J140038.9-025122

We examined FIRST J140038.9-025122 because it was noted as one of the 11 FRB-associated candidates by Ofek [2017]. The source was detected by NVSS, FIRST, and VLASS, but was not detected by GB6, VLSSr, TGSS, or a VLA observation from 1983 from the archives (Table 4.6). The light curve corrected for spectral index is visible in Figure 4.7. We can see that the FIRST detection was the highest flux observation, after which the source has been stable at a lower flux.

The host galaxy of the source is NGC 5400, which is 113.7±8.0 Mpc distant [de Vaucouleurs et al., 1991]. This distance allows us to calculate a luminosity at peak flux from the FIRST observation of $L = 2.0 \times 10^{28}$ erg s^{-1}Hz^{-1}. FIRST J140038.9-025122 is located in the spiral arm of a galaxy, 26.4" from the center.

Further, we identified Swift observations which overlapped with the field of FIRST J140038.9-025122. Although there was no source at this location, we can establish an upper limit at 0.2-10

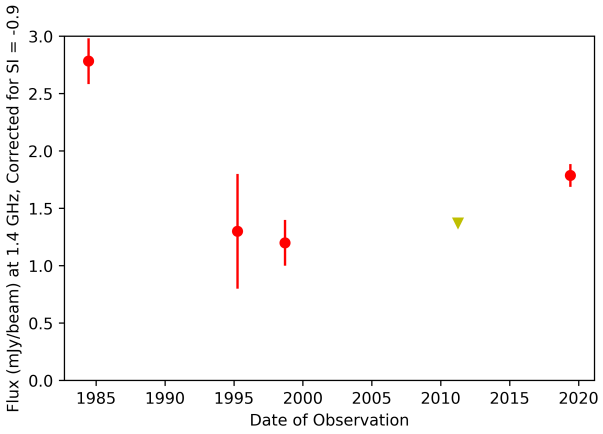

Figuur 4.7 As in Figure 4.2, but for FIRST J140038.9-025122.

keV of 1.0×10^{-3} ct/s (at 90% confidence).

Date of Observation	Peak Flux (mJy)	Observations	Frequency (GHz)
1984-06-10	2.6 ± 0.2	VLA AW0110	1.51
1995-02-27	1.3 ± 0.5	NVSS	1.4
1998-09-04	1.2 ± 0.2	FIRST	1.4
2003-09-20	<360	VLSSr	0.075
2011-03-01	<13	TGSS	0.15
2019-05-01	0.9 ± 0.1	VLASS	2-4

Tabel 4.6 Table of flux values over time for FIRST J140038.9-025122. All non-detections are listed as 3σ upper limits.

4.3.7 FIRST J114529.3+192327

We examined FIRST J114529.3+192327 because it was noted as one of the 11 FRB-associated candidates by Ofek [2017]. The source was detected by NVSS, FIRST, and VLASS, but was not detected by GB6, VLSSr, TGSS, or a VLA observations from 1983, 2000, and 2007 from the archives (Table 4.7). The light curve corrected for spectral index is visible in Figure 4.8. We can see that the FIRST detection was the highest flux observation, after which the source has been stable at a lower brightness. We can see that the source is brighter in VLASS than it was when it was detected in NVSS and FIRST, and underwent a period of non-detection in the interim.

The host galaxy of the source is NGC 3867, which is 104.8±7.87 Mpc distant [Smith et al., 2004]. This distance allows us to calculate a luminosity at peak flux from the FIRST observation of $L = 4.1 \times 10^{28}$ erg s^{-1}Hz^{-1}. FIRST J114529.3+192327 is located in the edge of a galaxy, 33.35" from the center.

Further, we identified Swift observations which overlapped with the field of FIRST J140038.9-025122. Although there was no source at this location, we can establish an upper limit at 0.2-10 keV of 1.5×10^{-3} ct/s (at 90% confidence). However, there is an X-ray source associated with

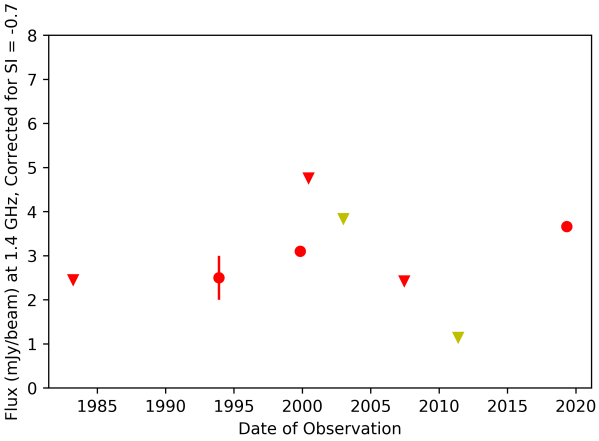

Figuur 4.8 As in Figure 4.2, but for FIRST J114529.3+192327.

FIRST J140038.9-025122. Identified by ROSAT as X-ray source 1RXS J140037.3-025103, the source has a count rate of $1.878 \times 10^{-02} \pm 9.164 \times 10^{-03}$ ct s^{-1} [Voges et al., 1999], and a flux of 4.800×10^{-13} erg cm^{-2}Hz^{-1} [Turriziani et al., 2007]. However, because the ROSAT positional error for this source is 25", and the source is in fact 31" distant from the galaxy, we conclude this is a coincident association.

Date of Observation	Peak Flux (mJy)	Observations	Frequency (GHz)
1983-03-12	<2.4	VLA O34	1.46
1987	<12.6	GB6	4.85
1993-12-06	2.5 ± 0.5	NVSS	1.4
1999-11-01	3.1 ± 0.1	FIRST	1.4
2000-06-15	<4.6	VLA AC540	1.5
2003-09-20	<279	VLSSr	0.075
2007-06-22	<2.4	VLA AC483	1.43
2011-04-15	<12	TGSS	0.15
2019-04-19	2.5 ±0.1	VLASS	2-4

Tabel 4.7 Table of flux values over time for FIRST J140038.9-025122. All non-detections are listed as 3σ upper limits.

4.3.8 FIRST J140255.7+092514

FIRST J140255.7+092514 is notable in our survey because of its extreme spectral index of $\alpha = -1.59$. The source was detected by FIRST, NVSS, VLASS, and a VLA observation from 1983, but was not detected by GB6, NVSS, VLSSr, or TGSS (Table 4.8). The light curve corrected for spectral index is visible in Figure 4.9. We can see that the source increased in brightness from 1983 to its detection in NVSS in 1983, but has decreased in brightness since.

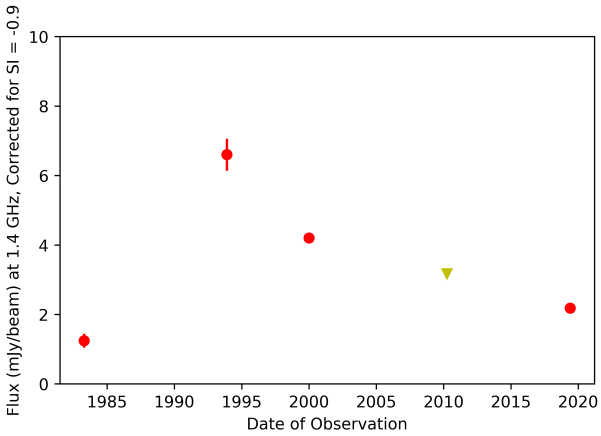

Figuur 4.9 As in Figure 4.2, but for FIRST J140255.7+092514.

The host galaxy of the source is NGC 5424, which is 87.1±6.2 Mpc distant [Falco et al., 1999]. This allows us to calculate a luminosity at peak flux from the FIRST observation of $L = 6.0 \times 10^{28}$ erg s^{-1}Hz^{-1}. FIRST J140255.7+092514 is located at the center of its host galaxy.

Further, we identified Swift observations which overlapped with the field of FIRST J140255.7+092514. Although there was no source at this location, we can establish an upper limit at 0.2-10 keV of 8.5×10^{-4} ct/s (at 90% confidence).

Date of Observation	Peak Flux (mJy)	Observations	Frequency (GHz)
1983-03-16	1.2±0.2	VLA AN0021	1.46
1987	<17	GB6	4.85
1993-12-06	6.6 ± 0.46	NVSS	1.4
2000-01-15	4.2 ± 0.1	FIRST	1.4
2003-09-20	<260	VLSSr	0.075
2010-02-28	<33	TGSS	0.15
2019-05-08	1.1±0.1	VLASS	2-4

Tabel 4.8 Table of flux values over time for FIRST J140255.7+092514. All non-detections are listed as 3σ upper limits.

4.3.9 FIRST J092758.2-022558

We examined FIRST J092758.2-022558 because it was noted as one of the 11 FRB-associated candidates by Ofek [2017]. The source was detected by NVSS, FIRST, and VLASS, but was not detected by VLSSr or TGSS (Table 4.9). The light curve corrected for spectral index is visible in Figure 4.10. We can see that the source has remained fairly steady in flux over this period.

The host galaxy of the source is CGCG 006-045, which is 108.4±7.8 Mpc distant [Jones et al., 2010]. This distance allows us to calculate a luminosity at peak flux from the NVSS observation of $L = 3.2 \times 10^{28}$ erg s^{-1}Hz^{-1}. FIRST J092758.2-022558 is located in the spiral arm of a galaxy, 14.3" from the center.

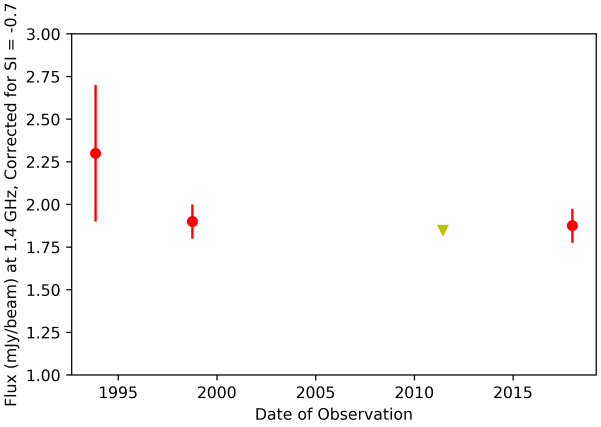

Figuur 4.10 As in Figure 4.2, but for FIRST J092758.2-022558.

Date of Observation	Peak Flux (mJy)	Observations	Frequency (GHz)
1993-11-15	2.3 ± 0.4	NVSS	1.4
1998-09-01	1.9 ± 0.1	FIRST	1.4
2003-09-20	<260	VLSSr	0.075
2011-06-15	<11	TGSS	0.15
2018-01-02	1.1±0.1	VLASS	2-4

Tabel 4.9 Table of flux values over time for FIRST J092758.2-022558. All non-detections are listed as 3σ upper limits.

4.3.10 FIRST J104726.6+060247

We examined FIRST J104726.6+060247 because it was noted as one of the 11 FRB-associated candidates by Ofek [2017]. The source was detected by NVSS, FIRST, VLASS, and TGSS, but was not detected by VLSSr (Table 4.10). The light curve corrected for spectral index is visible in Figure 4.11. We can see that the source has remained steady in flux over this period.

The host galaxy of the source is NGC 3376, which is 91.3±6.4 Mpc distant [Smith et al., 2004]. This distance allows us to calculate a luminosity at peak flux from the NVSS observation of $L = 2.7 \times 10^{28}$ erg s^{-1}Hz^{-1}. FIRST J104726.6+060247 is located away from the center of the galaxy, 5.9" from the center.

4.3.11 FIRST J235351.4+075835

We examined FIRST J235351.4+075835 because it was noted as one of the 11 FRB-associated candidates by Ofek [2017]. The source was detected by FIRST and VLASS, but was not detected by GB6, TGSS or VLSSr (Table 4.11). For the NVSS data, visual inspection confirmed the source was unresolved and had extended emission, so we did not include this data point in our study. The light curve corrected for spectral index is visible in Figure 4.12. We can see that the source has remained fairly steady during this period.

The host galaxy of the source is NGC 7782, which is 74.0±5.2 Mpc distant [de Vaucouleurs

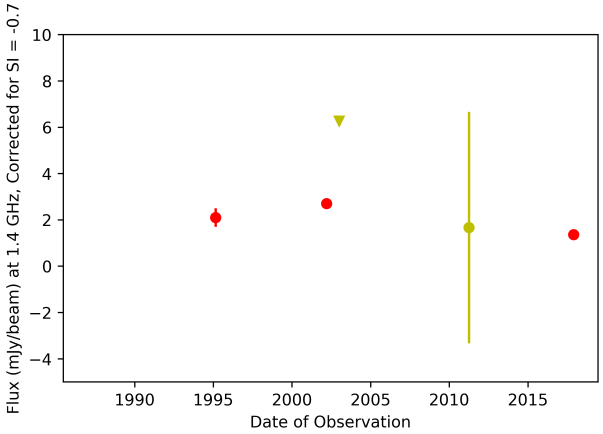

Figuur 4.11 As in Figure 4.2, but for FIRST J104726.6+060247.

Date of Observation	Peak Flux (mJy)	Observations	Frequency (GHz)
1987	<17	GB6	4.85
1995-02-27	2.1 ± 0.4	NVSS	1.4
2002-02-02	2.7 ± 0.1	FIRST	1.4
2003-09-20	<260	VLSSr	0.075
2011-02-28	19±7	TGSS	0.15
2017-11-22	0.8±0.1	VLASS	2-4

Tabel 4.10 Table of flux values over time for FIRST J104726.6+060247. All non-detections are listed as 3σ upper limits.

et al., 1991], which is an early-type spiral galaxy (type Sb) [Pignatelli et al., 2001]. We include an optical image of NGC 7782 with the position of FIRST J235351.4+075835 marked in Figure 4.13. This distance allows us to calculate a luminosity at peak flux from the FIRST observation of $L = 2.5 \times 10^{28}$ erg s^{-1}Hz^{-1}. We include an optical image of NGC 7782 with the position of FIRST J235351.4+075835 marked in Figure 4.13.

Further, we identified Swift observations which overlapped with the field of FIRST J235351.4+075835. Although there was no source at this location, we can establish an upper limit at 0.2-10 keV of 5.9×10^{-5} ct/s (at 90% confidence).

Date of Observation	Peak Flux (mJy)	Observations	Frequency (GHz)
1987	<13	GB6	4.85
2009-04-19	3.9 ± 0.1	FIRST	1.4
2003-09-20	<180	VLSSr	0.075
2010-06-15	<24	TGSS	0.15
2019-05-08	1.1±0.1	VLASS	2-4

Tabel 4.11 Table of flux values over time for FIRST J235351.4+075835. All non-detections are listed as 3σ upper limits.

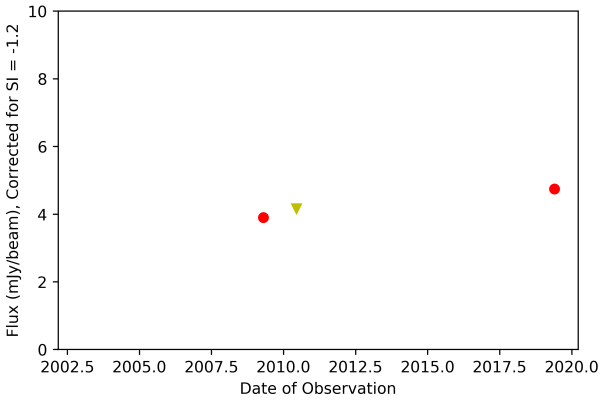

Figuur 4.12 As in Figure 4.2, but for FIRST J235351.4+075835.

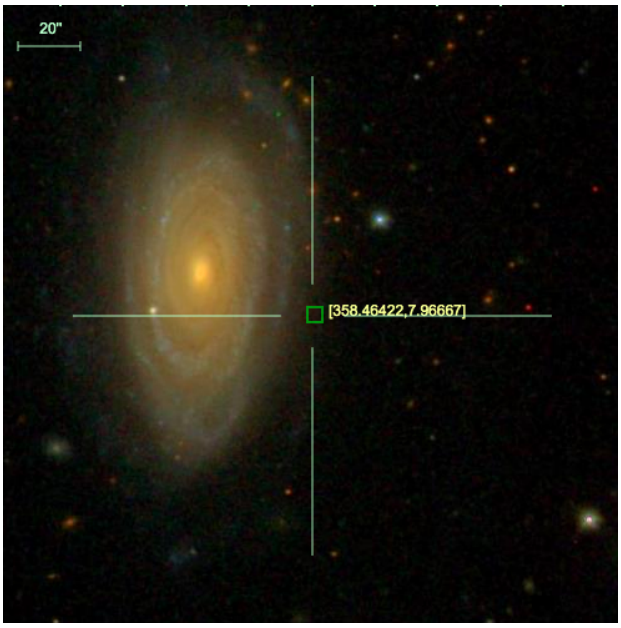

Figuur 4.13 The SDSS image for FIRST J235351.4+075835, including the host galaxy NGC 7782.

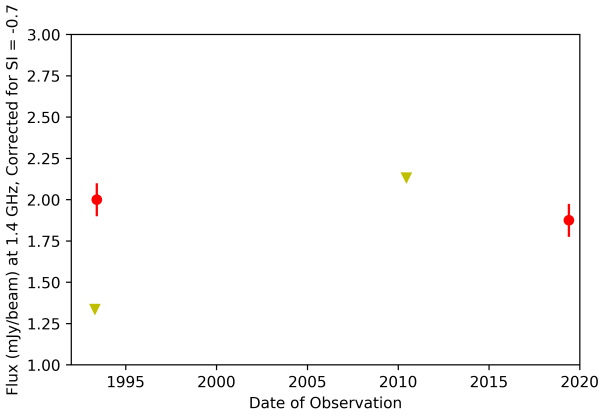

Figuur 4.14 As in Figure 4.2, but for FIRST J131441.9+295959.

FIRST J235351.4+075835 is near a spiral arm, 42.7" from the center of the galaxy. We identified one GRB coincident with this source's position, STK01 08530c, which was a non-triggered event identified after data re-analysis of BATSE data, occurring on October 1, 1991. While the coordinates for this GRB are 40 arcminutes from this source, the error circle for this event is 20.5 degrees. This large error circle means we chose to not associate this source with the GRB.

Further, we identified Swift observations which overlapped with the field of FIRST J235351.4+075835. Although there was no source at this location, we can establish an upper limit at 0.2-10 keV of 5.9×10^{-3} ct/s (at 90% confidence).

4.3.12 FIRST J131441.9+295959

We examined FIRST J131441.9+295959 because it was noted as one of the 11 FRB-associated candidates by Ofek [2017]. The source was detected by FIRST and VLASS, but was not detected by GB6, WENSS, TGSS or VLSSr (Table 4.12). For the NVSS data, visual inspection confirmed the source was unresolved and had extended emission, so we did not include this data point in our study. The light curve corrected for spectral index is visible in Figure 4.14. We can see that the source was not detected by WENSS, but increased in brightness dramatically by the FIRST observation, and has been at the same flux since assuming a spectral correction of -0.7. We also note that the WENSS data were taken at some point during the period of the 23rd of April 1993 and 20th of May 1993, and the FIRST observation was taken May 4, 1993.

The host galaxy of the source is CGCG 160-169, which is 104.8±7.3 Mpc distant [Berlind et al., 2006]. This distance allows us to calculate a luminosity at peak flux from the NVSS observation of $L = 5.0 \times 10^{28}$ erg s^{-1}Hz^{-1}. From the VLASS observation, we can calculate a luminosity of $L = 1.0 \times 10^{28}$ erg s^{-1}Hz^{-1}. FIRST J131441.9+295959 is located at the edge of a spiral galaxy, 20.6" from the galaxy center.

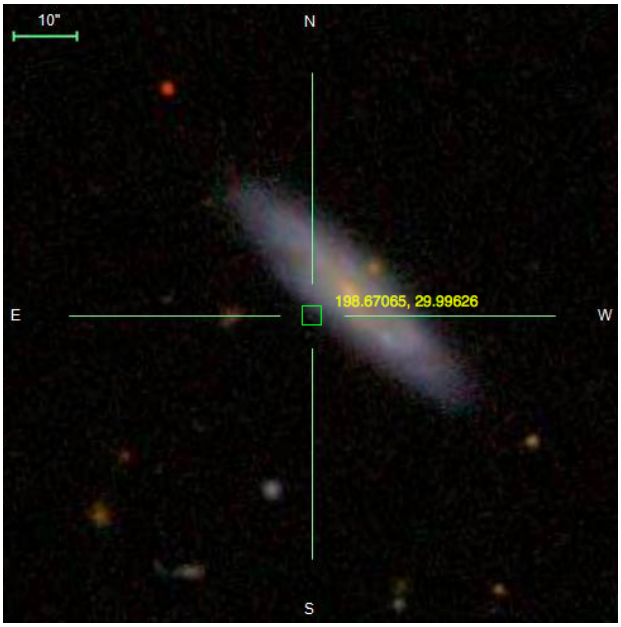

Figuur 4.15 The SDSS image for J131441.9+295959, including the galaxy CGCG 160-169.

Date of Observation	Peak Flux (mJy)	Observations	Frequency (GHz)
1987	<10	GB6	4.85
1993-04-23 to 1993-05-20	<6.5	WENSS	.325
1993-05-04	2.0 ± 0.1	FIRST	1.4
2003-09-20	<230	VLSSr	0.075
2010-06-15	<27	TGSS	0.15
2019-05-08	1.1±0.1	VLASS	2-4

Tabel 4.12 Table of flux values over time for FIRST J131441.9+295959. All non-detections are listed as 3σ upper limits.

4.3.13 FIRST J162244.5+321259

We examined FIRST J162244.5+321259 because it was noted as one of the 11 FRB-associated candidates by Ofek [2017]. The source was detected by NVSS, FIRST, and VLASS, but was not detected by GB6, TGSS, or VLSSr (Table 4.13). The light curve corrected for spectral index is visible in Figure 4.16. We can see that the source has been steadily decreasing in brightness over time.

The host galaxy of the source is 2MASS J16224461+3213007, which is 98.5±6.9 Mpc distant [Berlind et al., 2006]. This distance allows us to calculate a luminosity at peak flux from the NVSS observation of $L = 2.7 \times 10^{28}$ erg s^{-1}Hz^{-1}. FIRST J162244.5+321259 is located away from the center of the galaxy, 5.9" from the center.

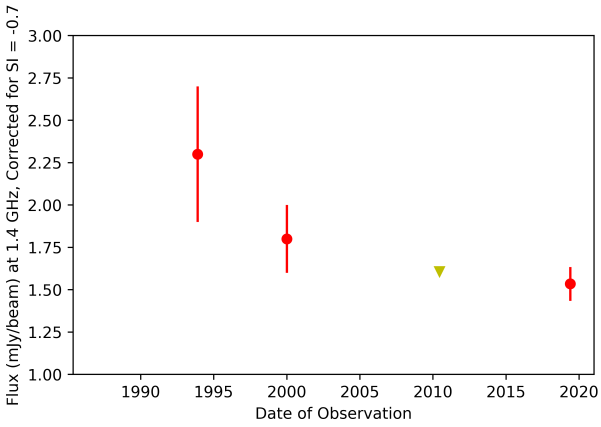

Figuur 4.16 As in Figure 4.2, but for FIRST J162244.5+321259.

Date of Observation	Peak Flux (mJy)	Observations	Frequency (GHz)
1987	<11	GB6	4.85
1993-12-06	2.3 ± 0.4	NVSS	1.4
2000-01-15	1.8 ± 0.2	FIRST	1.4
2003-09-20	<230	VLSSr	0.075
2010-06-15	<18	TGSS	0.15
2019-05-08	0.9±0.1	VLASS	2-4

Tabel 4.13 Table of flux values over time for FIRST J162244.5+321259. All non-detections are listed as 3σ upper limits.

4.3.14 FIRST J141420.8+073058

We examined FIRST J141420.8+073058 because we wanted to include a source with a positive spectral index in our data set. The source was detected by NVSS, FIRST, and VLASS, but was not detected by GB6, TGSS, or VLSSr (Table 4.14). The light curve corrected for spectral index is visible in Figure 4.17. We can see that the source has been varying in brightness over time- it was brightest when observed by NVSS, faintest during FIRST, and then has increased in brightness in VLASS.

The host galaxy of the source is NGC 5519, which is 113.6±8.0 Mpc distant [Hoffman et al., 1995]. This distance allows us to calculate a luminosity at peak flux from the NVSS observation of $L = 3.7 \times 10^{28}$ erg s^{-1}Hz^{-1}. FIRST J141420.8+073058 is located at the center of its galaxy.

4.3.15 FIRST J140031.1-025139

We examined FIRST J140031.1-025139 because we wanted to include a "typical" source in our sample which closely matched the expected spectral index for synchrotron radiation of $\alpha = -0.7$. The source was detected by NVSS, FIRST, and VLASS, and a VLA observation from 1984, but was not detected by GB6, TGSS, or VLSSr (Table 4.13). The light curve corrected for spectral index is visible in Figure 4.18. We can see that the source has been flat over time.

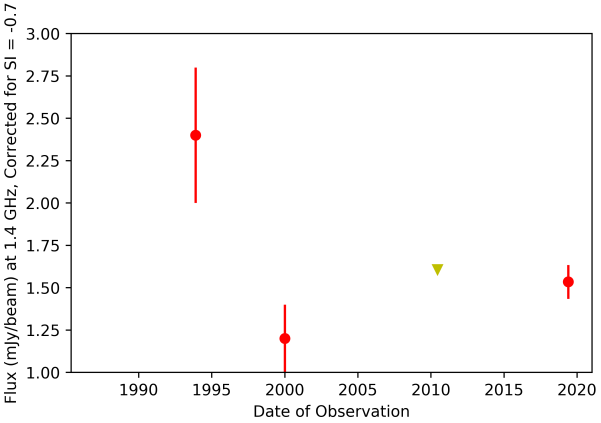

Figuur 4.17 As in Figure 4.2, but for FIRST J141420.8+073058.

Date of Observation	Peak Flux (mJy)	Observations	Frequency (GHz)
1987	<11	GB6	4.85
1993-11-15	2.4 ± 0.4	NVSS	1.4
1998-01-02	1.6 ± 0.1	FIRST	1.4
2003-09-20	<150	VLSSr	0.075
2010-06-15	<18	TGSS	0.15
2018-01-02	0.9±0.1	VLASS	2-4

Tabel 4.14 Table of flux values over time for FIRST J162244.5+321259. All non-detections are listed as 3σ upper limits.

The host galaxy of the source is NGC 5400, which is 113.7±8.0 Mpc distant [de Vaucouleurs et al., 1991]. This distance allows us to calculate a luminosity at peak flux from the NVSS observation of $L = 2 \times 10^{28}$ erg s^{-1}Hz^{-1}. FIRST J140031.1-025139 is located at the center of its galaxy.

Further, we identified Swift observations which overlapped with the field of FIRST J140031.1-025139. Although there was no source at this location, we can establish an upper limit at 0.2-10 keV of 1.0×10^{-3} ct/s (at 90% confidence).

4.3.16 FIRST J033623.0-005257

We examined J033623.0-005257 because it was not detected in the VLASS data. It was also not detected in NVSS data, to a 3σ upper limit of < 0.45 mJy/ beam, nor by VLA project AC0773 in March 2005 when it was <3 mJy/beam at 1.4 GHz. This radio source was detected in FIRST data with a radio flux of 1.3 ± 0.2 mJy/beam, and again in 2013-2014 during an observing campaign for transient radio sources at 3 GHz (VLA project code 13B-370; Kunal et al., in prep) when its flux was 0.571 ± 0.075 mJy (Table 4.16). There were also non-detections in VLSSr, GLEAM, and TGSS at low frequencies. We show the light curve of this radio source along with constraining non-detections in Figure 4.19, where we see the source was only detected during a increase in flux over a few years, and was not detected before or after these epochs.

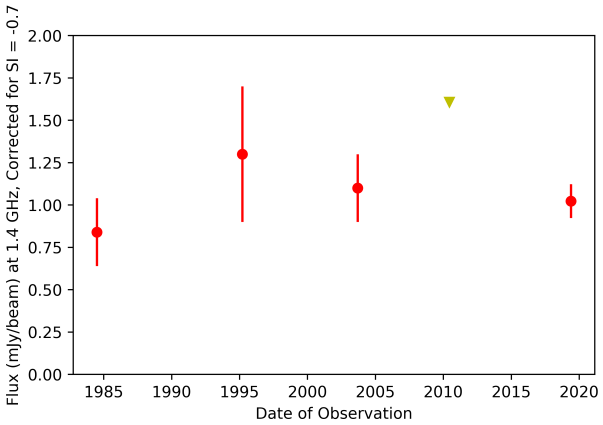

Figuur 4.18 As in Figure 4.2, but for FIRST J140031.1-025139.

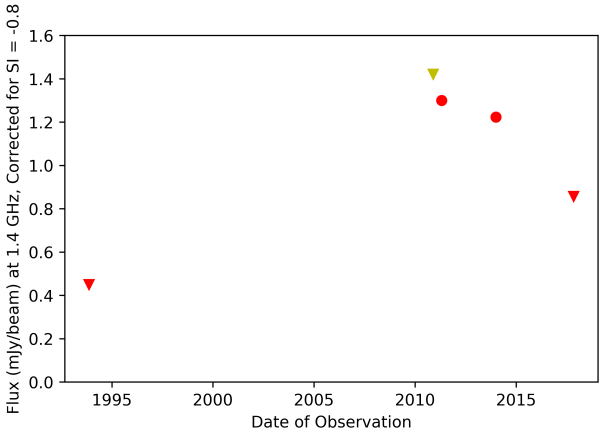

Figuur 4.19 As in Figure 4.2, but for FIRST J033623.0-005257.

Date of Observation	Peak Flux (mJy)	Observations	Frequency (GHz)
1984-06-23	1.2±0.2	VLA AN0021	1.46
1987	<210	GB6	4.85
1995-02-27	1.3 ± 0.4	NVSS	1.4
1998-08-09	1.1 ± 0.1	FIRST	1.4
2003-09-20	<360	VLSSr	0.075
2010-06-15	<18	TGSS	0.15
2019-05-01	0.6±0.1	VLASS	2-4

Tabel 4.15 Table of flux values over time for FIRST J140031.1-025139. All non-detections are listed as 3σ upper limits.

Date of Observation	Peak Flux (mJy)	Observations	Frequency (GHz)
1993-11-15	<0.45	NVSS	1.4
2003-09-20	<486	VLSSr	0.075
2005-03-26	<3	VLA AC0773	1.4
2010-12-14	<13	TGSS	0.15
2011-04-23	1.3 ± 0.2	FIRST	1.4
2013-08-09 to 2014-06-18	<37	GLEAM	0.118
2013-12-19 to 2014-01-14	0.57 ± 0.08	VLA 13B-370	3
2017-12-16	<0.4	VLASS	2-4

Tabel 4.16 Table of flux values over time for FIRST J033623.0-005257. All non-detections are listed as 3σ upper limits.

The position is coincident with the source 2MASX J03362300-0052576, classified as a Seyfert 1 galaxy at redshift z = 0.02 [Toba et al., 2014], and optical images confirm the radio source is coincident with the center of the galaxy (Figure 4.20).

Although the precise timescale is not known, our light curve indicates that FIRST J033623.0-005257 was visible for a period of years, and the optical association with the center of Seyfert galaxy 2MASX J03362300-0052576 allows us to calculate a luminosity at peak flux in FIRST of $L = 1.1 \times 10^{28}$ erg s^{-1}Hz^{-1}.

4.3.17 FIRST J025552.4+010409

The steepest spectral index in our sample was for source FIRST J025552.4+010409, and we show a summary of observed fluxes over time in Table 4.17. This source was first detected in 1993 in NVSS data, and was as bright as 2.8 ± 0.1 mJy in 1995 at 1.4 GHz when it was observed by FIRST as measured with Aegean, but was 0.8 ± 0.1 mJy in VLASS in 2017 at 3 GHz. If we use the flux measured directly from the FIRST image instead of the value obtained from the FIRST catalog (that is, 2.8 ± 0.1 mJy instead of 3.0 ± 0.14 mJy), we obtain a new spectral index of -1.6 (versus $\alpha = -1.8$ from the catalog value). The source was also detected in VLA observations by project 13B-370 (Kunal et al., in prep), and detected at low frequencies in 2011 by TGSS. We also found observations at these coordinates that were non-constraining upper limits, but include

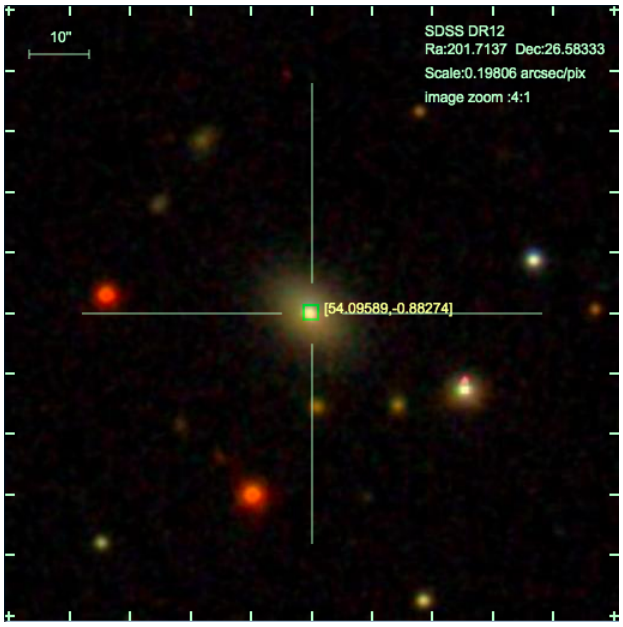

Figuur 4.20 The SDSS image for FIRST J033623.0-005257. This position is coincident with the source 2MASX J03362300-0052576, classified as a Seyfert 1 galaxy.

Date of Observation	Peak Flux (mJy)	Observation	Frequency (GHz)
1990-02-22	<1680	GB6	4.85
1993-11-15	1.5 ± 0.4	NVSS	1.4
1995-10-16	2.8 ± 0.1	FIRST	1.4
2006-06	<360	VLSSr	0.075
2010-12-12	7.0 ± 0.3	TGSS	0.15
2013-12-13 to 2014-01-14	0.82 ± 0.06	VLA 13B-370	3
2017-11-20	0.8 ± 0.1	VLASS	3

Tabel 4.17 Table of flux values over time for FIRST J025552.4+010409.

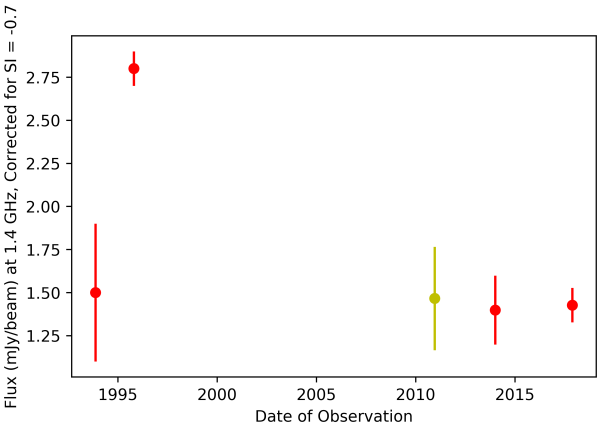

Figuur 4.21 As in Figure 4.2, but for FIRST J025552.4+010409.

Date of Observation	Peak Flux (mJy)	Observation	Frequency (GHz)
2002-3-24	2.1 ± 0.1	FIRST	1.4
2006-06	<366	VLSSr	0.074
2009-01-01 to 2009-01-03	1.81 ± .03	Stripe82	1.4
2010-10-31	<10.2	TGSS	0.15
2013-08-09 to 2014-06-18	<39	GLEAM	0.118
2013-12-13 to 2014-01-14	0.7 ± 0.07	VLA 13B-370	3
2017-11-30	0.6 ± 0.1	VLASS	3

Tabel 4.18 Table of flux values over time for FIRST J020203.2-000518.

them in Table 4.17 for completeness.

The light curve over time for FIRST J025552.4+010409 with the flux corrected for $\alpha = -0.7$ can be seen in Figure 4.21. We used this value for the correction because the 2006 TGSS detection at 150 MHz combined with the 2013 VLA observation are relatively close in time, and this allows us to find the spectral index more precisely than we did for our initial assumption. We found that the source was fairly flat, excepting the high flux measured by the FIRST survey.

Examination of SDSS images confirm that there is no optical galaxy at the coordinates for FIRST J025552.4+010409, although it does appear within 1 arcminute of an edge-on galaxy. Thus, it seems likely that FIRST J025552.4+010409 is at a distance >108 Mpc, and was included in the Ofek [2017] catalog due to chance coincidence. We can place a lower limit on the source's radio luminosity at 1.4 GHz of 4×10^{28} erg s^{-1}Hz^{-1}.

4.3.18 FIRST J020203.2-000518

FIRST J020203.2-000518 was identified due to its extreme variability between FIRST and VLASS observations. We list our compiled data over time in Table 4.18, and provide the light curve of data in Figure 4.22. When using the direct measurement of the flux from the FIRST image instead of the catalog value, we obtain a spectral index for this source of $\alpha = -1.5$. However, when compiling our data in Figure 4.22, we see the detections show a steady decay over ∼20

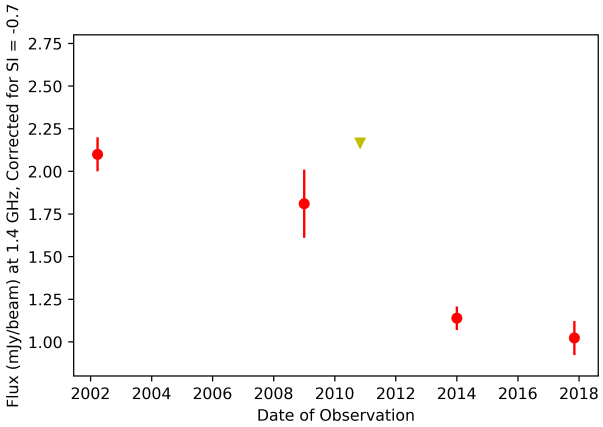

Figuur 4.22 As in Figure 4.2, but for FIRST J020203.2-000518 and corrected for a spectral index of $\alpha = -0.75$.

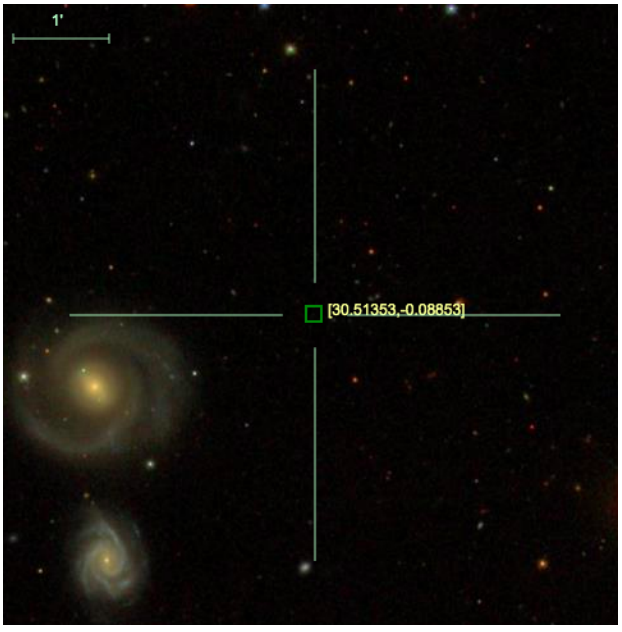

Figuur 4.23 The SDSS image for FIRST J020203.2-000518.

Date of Observation	Peak Flux (mJy)	Observation	Frequency (GHz)
1984-05-30	1.1 ± 0.4	VLA	1.51
1994-01-11	2.1 ± 0.4	NVSS	1.4
1995-11-13	1.1 ± 0.1	FIRST	1.4
2006-06	<360	VLSSr	0.075
2010-12-12	<10	TGSS	0.15
2017-11-25	0.6 ± 0.1	VLASS	3

Tabel 4.19 Table of flux values over time for FIRST J132651.2+263528.

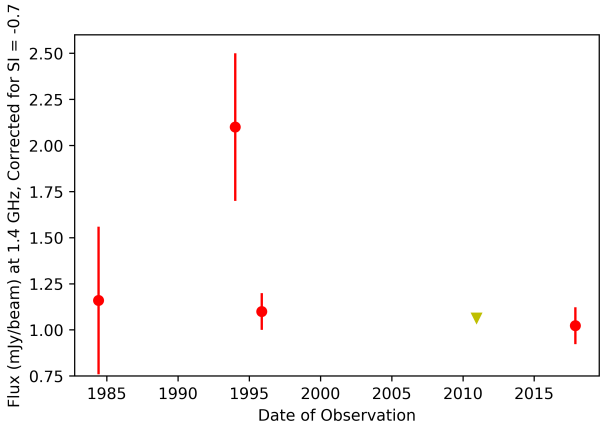

Figuur 4.24 Light curve for FIRST J132651.2+263528.

years, with one constraining non-detection in 2010 from TGSS data. We note that the source was also detected in NVSS, but was unresolved. If we calculate the upper limit for the spectral index when using this observation and the 2009 Stripe82 one, we obtain $\alpha \leq -0.7$.

We see in Figure 4.22 that the light curve consists of a steady decline over the ∼2 decades of observations since it was first detected. Similar to FIRST J033623.0-005257, we find that there is no optical counterpart to the coordinates of this radio source, and instead it is located ∼ 1 arcminute distant from a bright optical galaxy, NGC 799 (Figure 4.23). From this, we can calculate an upper limit its 1.4 GHz luminosity of $L_\nu = 2.6 \times 10^{28}$ erg s^{-1}Hz^{-1}, assuming a distance >108 Mpc.

4.3.19 FIRST J132651.2+263528

FIRST J132651.2+263528 was examined for two reasons: it matched our variability criteria, and the SDSS image for the source confirmed the radio source was near the center of the western of two interacting galaxies, 2MASS J13265127+2635285 and 2MASX J13265125+2635283. Collectively known as Markarian 454 [Mrk 454; Toba et al., 2014], they are undergoing what appears to be a merger process (Figure 4.25). Mrk 454 is located at a distance of 99 Mpc [Skrutskie et al., 2006], and the right (eastern) galaxy in Figure 4.25 is classified as an AGN [Toba et al., 2014].

The compiled data for this radio source can be found in Table 4.19, and the subsequent light curve in Figure 4.24. We can see in the light curve that this source increased in flux in NVSS

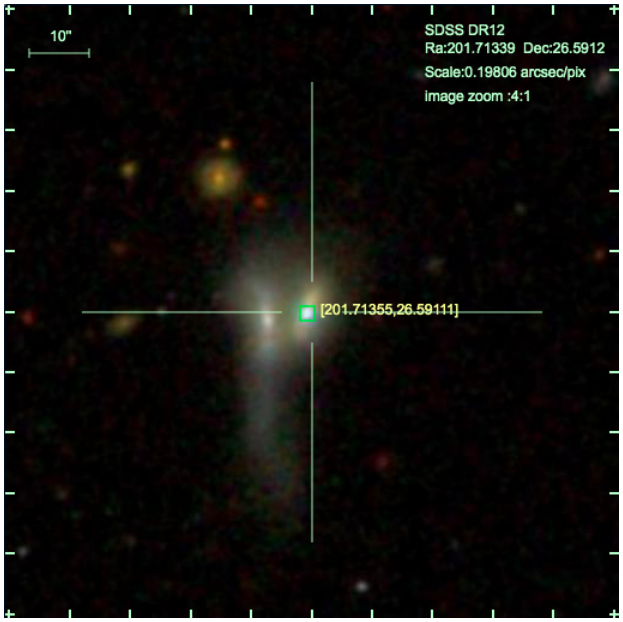

Figuur 4.25 The SDSS image for FIRST J132651.2+263528

data, where it was ∼2 times brighter than all other observations. Further, the source faded significantly in the 23 months between the NVSS and FIRST observations. When we used the directly measured peak flux from FIRST to recalculate the spectral index, we obtained $\alpha = -0.7$.

Because we know the distance to the galaxy, we can calculate the luminosity during this period of variability. We find that at its peak during the NVSS observation, the radio source at 1.4 GHz had a luminosity $L = 2.4 \times 10^{28}$ erg s^{-1}Hz^{-1}, which decreased by almost half to $L = 1.3 \times 10^{28}$ erg s^{-1}Hz^{-1} in ∼670 days.

Further, we identified Swift observations which overlapped with the field of FIRST J132651.2+263528. Although there was no source at this location, we can establish an upper limit at 0.2-10 keV of 1.0×10^{-3} ct/s (at 90% confidence). However, this radio source is also listed in Ofek [2017] as coincident with an X-ray source in the ROSAT catalog of count rate 1.1 ct/ks [1RXS J132640.4+263336; Voges et al., 1999]. However, because the ROSAT positional error for this source is 17", and the source is in fact 85"distant from the galaxy, and because we did not detect any counts from the Swift XRT data, we conclude this is a coincident association.

4.4 Discussion

Our study is important in the context of what we can learn about variability at local distances. In Section 4.4.1, we discuss the categorizations we used to identify our different radio sources. In Section 4.4.2, we cover the sources that we looked at in detail in Section 4.3, including a possible TDE or NS-NS merger candidate (Section 4.4.2.1), sources from low-excitation AGN activity (Section 4.4.2.2), and sources which exhibited non-transient behavior (Section 4.4.2.3. In Section 4.4.4, we compare the variability seen in our study to that seen in other surveys. In Section 4.4.3, we discuss the rate of NS-NS mergers with late time emission, as well as the local volumetric

rate of variable sources. In Section 4.4.5, we compare our sources to those of other transient phenomena in the local universe.

4.4.1 Categorizing Sources

From the information compiled in Section 4.3, we can consider the origins of those sources deemed worthy of further inspection. When categorizing the various sources in our study, we used three factors for each source:

- First, we considered the position of the source. This entailed noting whether the source was nuclear versus non-nuclear in its location within the galaxy, as a nuclear source is most likely to be associated with AGN related activity, or a TDE. We additionally noted if the source did not appear coincident with a galaxy, meaning the source was more likely to be a background source coincidentally included in our study. We also considered what X-ray information exists for the source, either from the lack of detection in the ROSAT catalog or a Swift XRT observation.
- Second, we were interested in the light curve over time for the source. In particular, we were interested in sources that displayed monotonic decay over time versus other behavior, such as flaring, which indicates different physical processes.
- Third, we were interested in whether the source underwent a large change in brightness during our survey. We defined these as sources which increased or decreased by a factor of two in flux during our study.

Once the sources were grouped together, we classified the likely source of emission based on the physical mechanisms underlying their origin. We found that none of the sources in our study met all three of our criteria. However, one source, FIRST J020203.2-000518 (Section 4.3.18), did display some of the criteria listed above, and may be confirmed as a transient with additional follow-up observations. We discuss all our sources in greater detail in Section 4.4.2 below.

4.4.2 Discussion of Individual Sources

4.4.2.1 Possible TDE or SGRB Candidate

FIRST J020203.2-000518 is notable because of its light curve (Figure 4.22). It has steadily decreased in brightness by a factor of ~ 2 since it was first detected in 1993 (assuming a synchrotron spectral index of $\alpha = -0.75$). We have calculated the decay rate of this source (Figure 4.26), and find a decay rate of $\beta = -0.6$ if we set the y-intercept for our fit t_0= 1993. We chose this value because an unresolved source was detected in NVSS at this position in 1993, but showed some extended emission via visual inspection of the data. Thus, we concluded that while we do not have the flux measurement from NVSS, it does seem likely it was already visible at that time. This combined with the monotonic decay leads us to conclude the light curve could be caused by a shocked CSM. Radio propagation phenomena, such as extreme scattering, are typically symmetrical in their light curves [Bannister et al., 2016; Fiedler et al., 1994] so we conclude this is less likely.

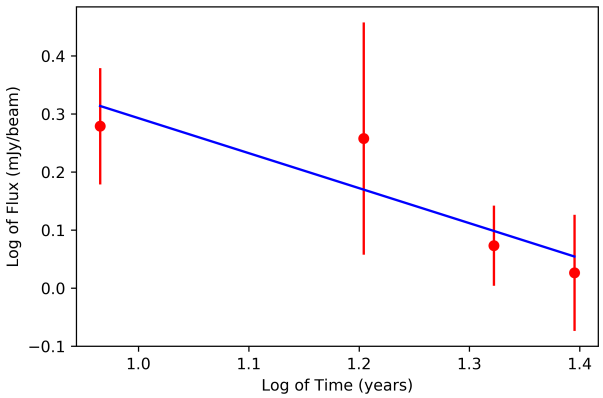

Figuur 4.26 A log-log plot of the flux over time for FIRST J020203.2-000518, assuming $t_0 = 1980$..

However, no optical counterparts coincided with the locations of the source. The reason it was included in the Ofek [2017] catalog is because the search radius from an optical galaxy was based on the optical galaxies galaxy's 25 mag arcsec^{-2} surface brightness semi-major axis listed in the HyperLEDA catalog, which could be very large in the event a nearby optical galaxy was also large. This resulted in an angular distance between the radio source and an optical galaxy for FIRST J020203.2-000518 of 183". If we assume a distance >108 Mpc, we can calculate an upper limit its 1.4 GHz luminosity of $L = 2.6 \times 10^{28}$ erg s^{-1}Hz^{-1}. However, if FIRST J020203.2-000518 is in fact located further, this would correspond with an even greater luminosity. Finally, it is notable that there has been a steady decrease in the light curve over the ∼25 years of data collected for this source, and we obtained an upper limit for X-ray emission from Swift XRT at 90% confidence of 0.2-10 keV of 1.0×10^{-3} ct/s.

We have first considered the possibility that the FIRST J020203.2-000518 source is at a much greater distance than its nearby galaxy host. Our upper limit on luminosity is much lower than what we would expect for an on-axis TDE, which is on the order of $10^{30} - 10^{31}$ erg s^{-1}Hz^{-1} [Metzger et al., 2015; Mooley et al., 2016]. However, an on-axis TDE has an expected light curve duration of ≤3 years at 1.4-3 GHz [Zauderer et al., 2013; Metzger et al., 2015], defined as the time interval over which the flux is within a factor of two of its peak value. If we assume that the NVSS observation occurred near the peak flux for a TDE event, it took >10 years to reach this value, making an on-axis TDE less likely. Although the details of the light curve for an off-axis TDE are not available, it is thought to last for years [Metzger et al., 2015], so this could still be a possible scenario for this event.

The second possibility we considered for FIRST J020203.2-000518 is that it is in fact associated with NGC 799 even though it appears 183" distant. If so, if we assume the source is at roughly the same distance of NGC 799 of distance of 83.2 ± 5.8 Mpc [Theureau et al., 1998], this would correspond with a distance between the center of the host and FIRST J020203.2-000518 of 73.8 kpc. While this exceeds the offsets observed for transients such as LGRB [Blanchard et al., 2016], up to 30% of NS-NS mergers are estimated to take place outside their host galaxies [Belczynski et al., 2006], and 25% of SGRB at ≥ 10 kpc [Fong & Berger, 2013]. Further, [Fong & Berger, 2013] reported the offset of GRB 090515 at 75.03 ± 0.15 kpc from its host galaxy, after using the

Hubble Space Telescope to conduct follow-up observations for counterpart galaxies in the burst's region. This leads us to the conclusion that it is possible that an SGRB occurred at the distance of FIRST J020203.2-000518 from NGC 799. If we assume FIRST J020203.2-000518 occurred at a distance of ∼83.2 Mpc, we find $L = 1.9 \times 10^{28}$ erg s^{-1}Hz^{-1}.

As such, we have considered whether the progenitor source for FIRST J020203.2-000518 could be related to a neutron star merger (NSM), either from an off-axis SGRB where the emission comes from the relativistic jet, or from the ejecta from the kilonova (KN) interacting with an ISM [Hallinan et al., 2017; Alexander et al., 2017; Berger, 2014; Nakar & Piran, 2011]. While the two phenomena are expected to have a similar expected luminosity of $10^{28} - 10^{29}$ erg s^{-1}Hz^{-1} [van Eerten et al., 2010; Metzger & Berger, 2012; Metzger et al., 2015], the radio emission from an off-axis SGRB peaks once the jet material sweeps up its own mass in ISM, whereas the radio emission from the KN ejecta peaks once it has swept up its own mass of ISM. Because the KN ejecta has a larger mass, it expands more slowly, and thus the radio emission takes longer to peak compared to the off-axis SGRB afterglow [Fong et al., 2016; Berger, 2014]. It is predicted that off-axis SGRB emission will peak after a few hundred days, whereas emission from the KN ejecta will peak closer to a decade after the NSM [see Figure 1; Metzger et al., 2015].

Our first concern in this scenario was whether the ISM at a distance of 73.8 kpc from the host galaxy would have a high enough density for corresponding radio emission. Although the ISM is expected to be low at such a distance, a smaller satellite galaxy is possible at these distances. Further, we note that SDSS images have a depth of g' ∼23 mag [York et al., 2000], and if placed at a distance of 83.2 Mpc even a Large Magellanic Cloud (LMC) sized satellite galaxy would not be detectable by SDSS. Therefore, such ISM levels are possible if the location of FIRST J020203.2-000518 is coincident with an unseen satellite galaxy of NGC 799.

A monotonically decreasing light curve of >20 years is more consistent with KN ejecta interaction compared to an off-axis SGRB [Metzger et al., 2015], leading us to conclude this scenario is the more likely of the two if FIRST J020203.2-000518 is located at this distance. However, while radio afterglows from SGRB have been observed [Hallinan et al., 2017; Fong et al., 2016], late-time emission from KN ejecta has not. It is predicted the emission would be highly dependent on the ISM density, and we should note a density of $n \leq 1$ cm^{-3} is the typical density scale inferred from existing SGRB observations [Fong et al., 2016, 2015]. Berger [2014] predicted emission from KN ejecta will peak at 0.15 mJy for a NSM located at 200 Mpc at 1 GHz, on a time scale of 10 years, assuming an ISM density $n = 0.1$ cm^{-3}. In the case of GW 170817, which occurred at a distance of $\sim$ 40 Mpc [Abbott et al., 2018], Alexander et al. [2017] predict emission will peak at $\leq 3\mu$Jy assuming the ISM is $n = 10^{-3}$ cm^{-3}. Both of these density estimates would correspond with luminosities far less than what we see from FIRST J020203.2-000518. Although it is possible the source is embedded in a relatively high density region in a faint satellite galaxy ($n \geq 1$ cm^{-3}), it is also likely to be in a region with very low ISM levels.

We conclude that we cannot definitively classify this transient candidate without additional optical and radio follow-up observations. In optical, such observations would be useful to determine whether there is a small galaxy at $\sim$ 83.2 Mpc distant (which may indicate NSM-related activity), or the center of a much larger galaxy at distance >108 MHz (indicating TDE-related activity). Radio observations in the future will also be useful in determining whether the monotonic

decrease in flux observed in this source continues.

4.4.2.2 AGN Candidates

We first considered the five variable radio sources which coincided with the center of their host galaxies. These are FIRST J143052.2+060209.6 (Section 4.3.1), FIRST J141430.5+060955.4 (Section 4.3.2), FIRST 140255.708+092514.54 (Section 4.3.8), FIRST 033623-005257 (Section 4.3.16), and FIRST J132651.2+263528 (Section 4.3.19). This is because nuclear transients are most likely associated with either AGN or TDE activity [Mooley et al., 2016; Tadhunter, 2016]. To distinguish between the two categories, we looked at the luminosities of the radio sources, which all had a peak luminosity at 1.4 GHz of $L_\nu \sim 10^{28}$ erg s^{-1}Hz^{-1}. This luminosity is fainter than that expected from a TDE, which occurs when a star gets sufficiently close enough to a black hole's event horizon that it is pulled apart by the black hole's tidal forces [Giannios & Metzger, 2011], and is typically associated with luminosities $\geq 10^{30}$ erg s^{-1}Hz^{-1} [Zauderer et al., 2013; Metzger et al., 2015]. We will also note that of these galaxies, only FIRST 140255.708+092514.54 had coincident X-ray observations, resulting in an upper limit of 8.5×10^{-4} ct/s (at 90% confidence).

However, this luminosity is consistent with that of a radio-loud AGN [Woo & Urry, 2002; Kimball et al., 2011]. Given the location of the sources at the center of their host galaxies, and the luminosities we observed, we conclude the variability we observed was due to flaring in the AGN. For example, for FIRST J132651.2+263528 (Section 4.3.19), located in one of the pair of interacting galaxies in Mrk 454, the light curve revealed a flare during the period observed by the NVSS survey (Figure 4.24). Further, the rightmost galaxy in Mrk 454 coinciding with the location of FIRST J132651.2+263528 is listed as an AGN. Finally, radio-loud AGN have been connected to interacting galaxies, which is thought to be triggered by the interactions. From this, we conclude this flare was likely related to AGN activity.

In the case of FIRST J025552.4+010409 (Section 4.3.17), no optical counterpart coincided with the locations of the source. The reason this source was included in the Ofek [2017] catalog is because the search radius from an optical galaxy was based on the optical galaxies galaxy's 25 mag arcsec^{-2} surface brightness semi-major axis listed in the HyperLEDA catalog, which could be very large in the event that a nearby optical galaxy was also large. This resulted in an angular distance between the radio source and an optical galaxy for FIRST J025552.4+010409 of 64". We also confirmed the location of this optical galaxy compared to their sources in SDSS data, and concluded it was a coincidental association.

Finally, we have a handful of sources which have a non-nuclear position that appears to be within a galaxy, and display some variability, but do not show monotonic behavior expected from transients. These sources are FIRST J140038.9-025122 (Section 4.3.6) and FIRST J114529.3+192327 (Section 4.3.7). They appeared at the edges of their respective galaxies, and show a peak luminosity of 10^{28} erg s^{-1}Hz^{-1}, but showed flaring behavior during the period of our study. Although many objects in our Local Group are known to flare (flare stars, pulsars, brown dwarfs, etc), all of these do not have sufficient luminosity to be detectable at these distances [see Table 1 of Mooley et al., 2016]. For example, magnetic flares from active binary stars do not exceed $10^{14} - 10^{22}$ erg s^{-1}Hz^{-1} [Güdel, 2002], and thus cannot explain our candidate signals. Finally, we will note that for both of these sources we obtained upper limits from Swift

XRT observations of the area, indicating neither is likely to be a site associated with high-energy phenomena.

Instead, we are left with two possibilities: that these light curves were caused by interstellar scattering (ISS), or a coincident background. If the variations we observed in these sources are due to ISS, this implies a compact source or component that is being refracted by a turbulent, ionized ISM. Together with the spectral index observed, this implies a classification as a compact steep spectrum source (CSS). Such sources have been detected by transient surveys in the past [Bannister et al., 2011]. Additional spectral information on these sources would help confirm these sources as CSS. Alternatively, these flares could be caused by coincident AGN that are background sources to the host galaxies.

Ultimately, we conclude AGN activity is the most reasonable remaining interpretation for all the variable sources covered in this section because they appear to be inconsistent with other possibilities for transients and variable sources. Given that many of these sources were primarily associated with the nuclei of galaxies, that AGN activity is the most common slow radio transient phenomenon at these frequencies that can be seen on time scales of decades, and that it is thought that all AGN may exhibit variability at some point [Tadhunter, 2016], and radio sources in the local universe are dominated by AGN [Nyland et al., 2016], this is unsurprising. Further, we should note that variability at 1 GHz from AGN is greatest on time scales of 2-5 years [Hancock et al., 2018; Bannister et al., 2011]. In a survey of 159 AGN flares at 22 and 37 GHz, Hovatta et al. [2008] found that the flares last on average 2.5 years and are only slightly longer at lower frequencies, which is also consistent with our observations. Some of our AGN candidates varied on longer periods of >10 years (see FIRST J033623.0-005257, Figure 4.22, for one such example), which has been noted in the past for other variable sources discovered in studies of transient and variable sources as well [Bannister et al., 2011; Mooley et al., 2016]. It is likely that these changes in variability are due to episodes of enhanced accretion onto the black hole, leading to increased jet activity in the AGN [Kunert-Bajraszewska et al., 2006; Frank et al., 2016].

We have also considered how our examined sources fit into what is known about the local AGN population. Best & Heckman [2012] conducted a study of nearby AGN ($z \leq 0.1$) using both SDSS optical spectra and NVSS and FIRST radio data, and found the local galaxy population is dominated at luminosities $L < 10^{33}$ erg s^{-1} Hz^{-1} by 'low-excitation' radio galaxies (LERG), which have very little radiated energy, as opposed to the quasar-like 'high-excitation' radio galaxies (HERG). The emission in LERG is thought to be from advection-dominated accretion flows which are optically thin, whereas HERG emission is driven by a radiatively efficient, optically thick accretion disc [Shakura & Sunyaev, 1973]. It should also be noted that HERG emit radiation over a very broad part of the electromagnetic spectrum, including X-rays, but LERG do not show accretion-related X-ray emission [Elvis et al., 1994; Hardcastle et al., 2007]. Finally, morphological radio studies of low radio luminosity galaxies show most of these sources are compact and lack prominent jets or diffuse lobes [Baldi et al., 2015], which is similar to what we found in our sources.

None of our sources were detected in the ROSAT catalog, which had a brightness limit of 0.1 cts/s at the 0.1- 2.4 keV energy band [Voges et al., 1999], although we have deeper limits for the sources for which Swift observations exist. The lack of X-ray emission combined with the luminosities of our sources ($L \approx 10^{28}$ erg s^{-1} Hz^{-1}) lead us to conclude all our sources categorized

as AGN are LERG. Our detected radio emission in this situation originates from radiatively inefficient flows that have low accretion rates, and changes in variability are due to the changes in density within these flows.

4.4.2.3 Non-Varying Sources

Finally, we will note that eight of our sources- FIRST J102526.1 +171547 (Section 4.3.4), FIRST J105823.6 +241355.3 (Section 4.3.5), FIRST J092758.2 -022558 (Section 4.3.9), FIRST J104726.6+060247 (Section 4.3.10), FIRST J235351.4 +075835 (Section 4.3.11), FIRST J131441.9 +295959 (Section 4.3.12), FIRST J162244.5 +321259 (Section 4.3.14), and FIRST J141420.8 +073058 (Section 4.3.15)- did not meet our criteria as a variable candidate as outlined in Section 4.2.3, and did not meet more than one of our criteria outlined above in Section 4.4.1. Further, in the case of FIRST J141420.8+073058 and FIRST J235351.4+075835, Swift XRT data indicated these sources are not associated with X-rays, and are unlikely to be a high-energy sources. For the sources located at the center of their galaxies (FIRST J162244.5+321259 and FIRST J141420.8+073058), we conclude this emission is likely caused by LERG behavior. The remainder of our sources are also likely due to non-transient emission, from either a local source to the host galaxy such as star formation, or an AGN at greater distance.

4.4.3 Rates

4.4.3.1 NSM Merger Afterglow

Based on our identification of FIRST J020203.2-000518 as a possible NSM candidate, We have calculated the volumetric rate of NSM afterglows detectable in radio, assuming these transients scale with stellar luminosity at distances < 108 Mpc. If we consider sources where $\Delta t_{1.3} = 4000$ days- the longest light curve duration predicted by Metzger et al. [2015] for a NSM- we can use the relationship:

$$R_{var} \approx \frac{1 \text{ event}}{\Delta t \; f_{spec} \; \Delta\Omega (d^3/3)} \tag{4.3}$$

where f_{spec} is the estimated completeness of stellar luminosity in the catalog to this distance [$\sim$30%; Ofek, 2017], and $\Delta\Omega$ is the footprint of the area of sky covered by the FIRST catalog of 10,600 deg^2. From this, we obtain a rate of $\sim$200 Gpc^{-3}yr^{-1}. This is lower than the rate predicted for NS-NS mergers predicted by Abbott et al. [2017] of 1540^{-1120}_{+3200} Gpc^{-3}yr^{-1}, based on the single detection of GW 170817 during the O1 and O2 LIGO science runs. However, we emphasize that the fraction of NS-NS mergers with emission at later times is not yet well established. For example, Nakar et al. [2006] predicted a local SGRB rate of $<$10 Gpc^{-3}yr^{-1} within 100 Mpc, but noted this rate could be several orders of magnitude higher based on factors such as the luminosity function and beaming factor. Further, we know any future KN emission from GW 170817 will be difficult to detect with current instruments [Alexander et al., 2017].

In the future, we expect LIGO will allow us to obtain a more precise rate of NS-NS mergers, both in the local surroundings and at greater distances, especially as the O3 science run is currently ongoing [Abbott et al., 2018]. While GW 170817 was nearby, analysis has suggested that GRB 170817A-like events are rare in the existing SGRB catalogs, and just a few percent of

NS-NS mergers may have accompanying emission [Mandhai et al., 2018], which may explain the discrepancy between our rate and the Abbott et al. [2017] rate of NSM. Detecting more decaying light curves like FIRST J020203.2-000518 may pay a key role in establishing the true rates of radio transients. It would also be useful for when the Square Kilometer Array (SKA) comes online, which is expected to find many more transients, in order to establish long-term transient behavior.

4.4.3.2 Local Volumetric Rate of Variable Sources

We have also obtained a local volumetric rate of variability based on our survey. Using Equation 4.3, if we use the 10 sources that fit the variability statistic in Equation 4.2, we obtain a rate of $\sim$4100 $\mathrm{Gpc^{-3}yr^{-1}}$.

As noted in Section 4.3, two sources that matched $V_s \geq 4.3$ do not have an associated host galaxy. Although it is possible that some of these sources are from transients that were kicked out of their host galaxy systems [Fong & Berger, 2013], it is more likely that the radio source is a false association between the galaxy and a coincident AGN at >108 Mpc. Thus, if we restrict the calculation to radio sources with an optical counterpart that have a high variability statistic, we are left with a rate of $\sim$3300 $\mathrm{Gpc^{-3}yr^{-1}}$.

4.4.4 Comparing Variability in Surveys

We have compared our rate of radio variability to other surveys. Hodge et al. [2013] conducted a study of variability for mJy sources in Stripe 82 [Hodge et al., 2011], and established that 1% of sources had a fractional variability $f_{var} < 3$ between 7 and 22 years. They concluded a majority of these sources were due to AGN. More recently, Mooley et al. [2016] established a variability fraction >4% on time scales of 1.5 years. In our survey, 3% of the sources varied by this amount over the $\sim$25 years of our study, which is consistent with the prevailing view that only a few percent of the sources in the radio sky are variable. In coming years, VLASS will cover the sky at two more epochs, which will allow us to continue monitoring variability in these sources.

At lower frequencies, Bell et al. [2019] have reported on the variability rate of bright (> 4 Jy) radio sources at 154 MHz using the MWA. They found that $\sim 1.6\%$ of radio sources display variability at time scales > 2.8 years, and concluded that this variability is due to interstellar scintillation. They also concluded that synchrotron-driven variability and intrinsic AGN variability can only produce changes at low frequencies on >100 year time scales. As such, it is not clear whether we can draw conclusions on radio observations of these sources at lower ($\sim$100 MHz) frequencies compared to our GHz frequencies on the time scale of our study.

We have also considered the biases inherent in using data from different studies to compile our light curves. One such consideration is that some of our variables could be artificial and due to angular resolution differences between the various surveys we used, particularly if diffuse components were present. For comparison, NVSS had a beam size of 45änd was observed in D configuration [Condon et al., 1998], FIRST had a beam size of 5änd was observed in B configuration [Becker et al., 1994], and VLASS has a beam size of 2.5änd was observed in configurations B and BnA [Lacy et al., 2019]. This means that VLASS and FIRST are missing short spacings compared to NVSS, and because VLASS was taken at a higher frequency compared to NVSS and

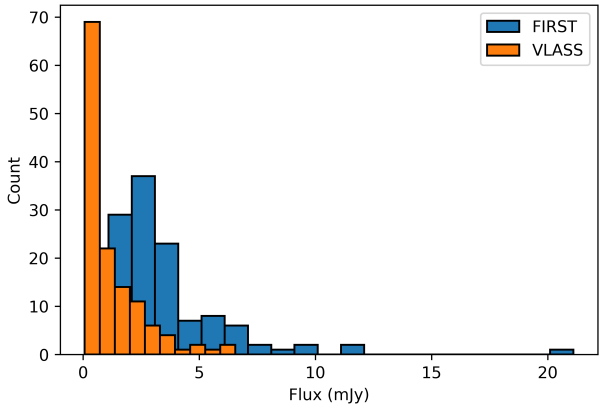

Figuur 4.27 A histogram of flux values for all the sources from Ofek [2017] observed by FIRST (blue), and a histogram of the same values from this study and Law et al. [2018] (yellow). The outlying data point in the FIRST data at ∼20 mJy is FIRST J141919+394036, and the second brightest source is FIRST 105823.641+241355.32.

FIRST (2-4 GHz instead of 1.4 GHz, respectively). It is thus conceivable that this discrepancy can make a source clearly detected in NVSS to appear to fade or disappear altogether in VLASS, even though it has not faded in actuality. Further, due to the differences in resolution it is possible that several radio sources close together would appear as a brighter radio source in NVSS, yielding a bright flux from that observation, but be resolved into multiple sources in a later survey where each appears fainter. We in fact found this to be the case for several sources, both via visual inspection of the images and when examining the 2D Gaussian fit of the source finder and seeing whether the fit exceeded the beam size, indicating an unresolved source. Future studies which compare data from multiple surveys will need to take care when examining observations from different surveys, and how the observations are compared to one another.

4.4.5 Comparison to Other Transient Sources

4.4.5.1 Candidate LGRB FIRST J141919+394036

We can compare our estimated rate of variability to that derived by Law et al. [2018] for decades-long extragalactic radio transients which was derived using the same catalog yielding a volumetric rate assuming $\Delta t = 2000$ days of ∼900 $\mathrm{Gpc}^{-3}\mathrm{yr}^{-1}$. As this value was obtained when only half the sky had been surveyed by VLASS, and we found no transients of this time scale in the second half of the VLASS data, we can update the number of such transients to 450 $\mathrm{Gpc}^{-3}\mathrm{yr}^{-1}$. We conclude that the rate of variable events is in excess of transient events, although more precise rates will require a more analytic approach to a large fraction of VLASS data (Dykaar et al., in prep).

Beyond the occurrence rate, we can also consider how unique the disappearing radio source FIRST J141919+394036 was as an event by comparing it to sources from our study. First, the spectral index limit of FIRST J141919+394036 obtained between FIRST and VLASS is far lower than any we found in our study at $\alpha < -5.1$, and the steepest spectral index we found for one

object was -1.8 (Section 4.3.17). Furthermore, the source that we found missing in VLASS in our study (Section 4.3.16) had a much smaller limit on spectral index, $\alpha < -1.3$.

In simplest terms, this difference in spectral indices is from a bias towards bright sources in FIRST in the design of this transient study. FIRST J141919+394036 had a flux of 20.1 mJy [Law et al., 2018], meaning it was twice as bright in FIRST as any source we measured in VLASS (or, in fact, any other source covered in the full catalog). We provide a visualization of this in Figure 4.27, where we show a histogram of all the FIRST and VLASS flux values for sources in the full Ofek [2017] catalog that were in epoch 1.1 of VLASS. This shows that the discovery of FIRST J141919+394036 was somewhat serendipitous due to the luminosity of the source ($L \approx 7 \times 10^{29}$ erg s^{-1} Hz^{-1}).

Additionally, we note that we may have introduced a bias when correcting our fluxes for a spectral index of -0.7 when calculating variability. This is because if a source has a spectrum of ($\alpha < -0.7$), its calculated spectral index would appear less steep, meaning it might be excluded from our variability criteria. In the future, when multiple VLASS epochs can be compared for transients which will have the same frequency as well as beam size, these biases will be minimized.

4.4.5.2 AGN and FRB Connections

Since the theory of what mechanism causes FRBs is unknown– or even if there are multiple mechanisms– it is not unexpected that there have been efforts to link the origins of FRBs to AGN [Vieyro et al., 2017; Katz, 2017]. This has been particularly interesting as the large and variable rotation measure observed in the FRB 121102 bursts has only been observed to date in the vicinity of black holes [Michilli et al., 2018]. The association between FRBs and AGN is difficult to establish, however, due to the variable nature observed in many AGN [Williams & Berger, 2016; Vedantham et al., 2016].

Vieyro et al. [2017] recently proposed a model for FRBs in which the FRB signals originate from a turbulent plasma hit by a relativistic jet from an AGN. They predicted that this would result in a luminosity at 1.7 GHz of approximately 10^{30} erg s^{-1} Hz^{-1}, which would far exceed luminosities visible in our study. To date, however, we note that the FRB with the lowest dispersion measure (DM), FRB180729.J1316+55, has an estimated distance of ∼300 Mpc, assuming standard cosmological parameters [CHIME/FRB Collaboration et al., 2019].[3] This means that no FRB has as yet been detected from within the local distances covered in this survey. However, the prodigious rate of FRB detection by the Canadian Hydrogen Intensity Mapping Experiment (CHIME) leaves us optimistic that a FRB within this distance will be detected soon. If it does, we expect that the methods used in this study to compile information on a local counterpart's light curve over several decades will be of interest, and we expect that radio catalogs and archival data sets are complete enough that any variability over decades-long time scale could be established.

4.5 Conclusions

We have conducted a survey of 117 radio sources in VLASS that also appeared in the FIRST catalog, and were first listed by Ofek [2017] as potential counterparts to FRBs. We have identified

[3]Distance is from http://www.frbcat.org; see Petroff et al. [2016] for more info.

FIRST J020203.2-000518 as a transient candidate based on its luminosity, monotonic decay, and time scale of the signal, either as a NS-NS merger remnant if at closer distance, or a TDE if at a distance >108 Mpc. Additional optical follow-up observations are needed to confirm the location of this radio source and classify it further, as well as radio observations for long-term monitoring of this transient.

In addition to these sources, we compiled detailed light curves for 18 other sources, but conclude that all are likely related to normal AGN activity and variability. We conclude that the majority of slow transients in the local radio sky at GHz frequencies are AGN, with more exotic phenomena comprising only a small handful of the transients at this distance, and the majority of low luminosity AGN sources at these distances are due to LERGs with low, inefficient accretion rates. We estimate the local rate of variability for luminous radio sources to be $\sim$4100 $\mathrm{Gpc^{-3}yr^{-1}}$. We also expect that in the future, when nearby transient radio phenomena are discovered, the existing archives of radio data will prove useful in compiling the behavior of such sources before the event, in order to establish any prior variability.

4.6 Acknowledgements

We thank Huib Intema for his correspondence regarding TGSS data, Joseph Callingham for his assistance with providing the WENNS observation dates, and Kunal Mooley and Gregg Hallinan for their assistance with providing VLA 13B-370 fluxes. This research has made use of data obtained through the High Energy Astrophysics Science Archive Research Center Online Service, provided by the NASA/Goddard Space Flight Center. The National Radio Astronomy Observatory is a facility of the National Science Foundation operated under cooperative agreement by Associated Universities, Inc. The Dunlap Institute is funded through an endowment established by the David Dunlap family and the University of Toronto. C.J.L. acknowledges support from the National Science Foundation under grant 1611606. B.M.G. acknowledges the support of the Natural Sciences and Engineering Research Council of Canada (NSERC) through grant RGPIN-2015-05948, and of the Canada Research Chairs program.

RA (J2000)	Dec) (J2000)	FIRST Flux (mJy/beam)	NVSS Flux (mJy/beam)	VLASS Peak Flux (mJy/beam)	Spectral Index Spectral Index
*09:27:58.282	-02:25:58.95	1.9 ± 0.1		1.1 ±0.1	-0.7
*10:25:26.189	17:15:47.97	2.6 ± 0.1		1.0 ±0.1	-1.0
*10:47:26.693	06:02:47.72	2.7 ± 0.1	2.4±0.4	0.8 ±0.1	-1.6
*10:58:23.641	24:13:55.32	2.1 ± 0.2		0.7 ±0.1	-1.4
*11:45:29.346	19:23:27.46	3.1 ± 0.2	2.4±0.4	2.5 ±0.1	-0.3
*13:14:41.932	29:59:59.19	2.0 ± 0.1	4.0±0.5	1.1 ±0.1	-0.7
*14:00:38.929	-02:51:22.79	1.2 ± 0.2		0.9 ±0.1	-0.4
* 14:10:43.667	08:59:29.96	2.6 ± 0.2	4±0.4	3.4 ±0.1	0.3
*16:22:44.571	32:12:59.28	1.8 ± 0.2	2.7±0.4	0.9 ±0.1	-0.9
*23:53:51.412	07:58:35.91	3.9 ± 0.1		1.1 ±0.1	-1.6
00:06:28.516	-03:42:58.83	2.4 ± 0.2	2.3±0.4	4.1 ±0.1	-0.6
00:17:27.498	-09:34:26.56	2.5 ± 0.2		5.5 ±0.1	0.0

00:17:59.547	-09:16:00.89	1.6 ± 0.2	2.9±0.5	1.1 ±0.1	-0.9
00:21:51.145	-09:29:32.2	3.3 ± 0.2	5.1±0.5	2.3 ±0.1	-0.5
00:42:39.26	02:44:14.17	3.3 ± 0.1	5±0.5	2.1 ±0.1	-0.6
01:44:43.099	-04:07:46.25	5.2 ± 0.1	10.9±0.6	4.0 ±0.1	-0.2
*02:02:03.248	00:05:18.72	2.1 ± 0.1		0.6 ±0.1	-1.6
02:17:04.793	01:14:39.44	11.1 ± 0.2	11.9±0.6	0.7 ±0.1	-1.2
02:36:23.588	00:42:31.55	1.9 ± 0.1		5.7 ±0.1	-0.7
02:52:42.189	-08:48:15.76	3.1 ± 0.2	4.4±0.5	1.9 ±0.1	-0.1
02:52:51.841	-01:16:29.31	3.1 ± 0.2	5.4±0.6	2.4 ±0.1	-0.1
*02:55:52.403	01:04:09.95	3.0 ± 0.1		0.8 ±0.1	-1.7
*03:36:23.014	00:52:57.85	1.6 ± 0.1		<0.4	<1.8
07:54:26.555	16:13:5.27	9.8 ± 0.1	10.5±0.5	6.6 ±0.1	-0.4
07:58:0.444	52:51:42.18	6.3 ± 0.1	7±0.5	3.3 ±0.1	-0.6
07:59:57.145	35:48:51.54	6.1 ± 0.2	9.2±0.5	2.3 ±0.1	-1.0
07:59:17.875	27:04:40.32	1.8 ± 0.1		1.8 ±0.1	-0.0
08:33:30.775	41:31:31.89	2.9 ± 0.1	2.7±0.4	1.7 ±0.1	-0.5
08:50:56.603	36:20:7.65	1.9 ± 0.2	3.4±0.4	1.0 ±0.1	-0.6
09:16:41.894	30:54:55.35	1.9 ± 0.1		1.7±0.1	-0.1
09:19:45.473	33:44:42.28	3.7 ± 0.1	5±0.4	3.3 ±0.1	-0.1
09:20:02.17	01:02:17.82	11.4 ± 0.2	10.7±0.5	2.8 ±0.1	0.2
09:20:36.948	33:04:29.06	3.2 ± 0.1	4.4±0.4	1.1 ±0.1	-1.1
09:39:17.261	36:33:44.17	4.8 ± 0.2	4±0.4	2.5 ±0.1	-0.6
09:43:2.176	37:49:23.37	2.4 ± 0.1	2.4±0.4	1.1 ±0.1	-0.8
09:47:10.836	23:30:51.86	2.3 ± 0.1		2.3 ±0.1	-0.0
09:50:0.613	37:34:31.4	1.7 ± 0.2	2.8±0.5	0.8 ±0.1	-0.7
09:52:46.77	30:02:20.16	3.8 ± 0.1	3.1±0.4	1.7 ±0.1	-0.1
09:58:40.109	28:52:38.98	3.5 ± 0.2	2.4±0.4	2.6 ±0.1	-0.3
10:11:07.608	46:54:56	3.2 ± 0.2	3.9±0.4	1.8 ±0.1	-0.6
10:13:47.92	38:40:32.19	2.4 ± 0.2	2.8±0.4	1.3 ±0.1	-0.6
10:13:51.543	38:47:2.29	6.2 ± 0.1	3.7±0.4	3.6 ±0.1	-0.5
10:15:1.568	39:39:48.41	1.9 ± 0.1		1.4 ±0.1	-0.5
10:27:25.021	01:14:30.82	3 ± 0.1	3.1±0.4	0.7 ±0.1	-1.4
10:37:22.113	37:04:39.35	2.9 ± 0.1	4.7±0.5	1.9 ±0.1	-0.4
10:37:37.903	37:27:20.27	2.2 ± 0.1	3.4±0.5	1.1 ±0.1	-0.6
10:41:52.953	21:15:9.35	3.1 ± 0.2	2.5±0.4	1.3 ±0.1	-0.9
10:44:18.973	52:46:12.56	7.9 ± 0.1	5.4±0.4	2.7 ±0.1	-0.7
10:44:38.235	56:22:11.18	4.5 ± 0.2	5.2±0.4	2.7 ±0.1	-0.7
10:51:26.328	08:17:55.3	2.2 ± 0.1	2.4±0.4	3.0 ±0.1	-0.1
10:55:6.921	40:34:0.91	2.4 ± 0.1		3.5 ±0.1	0.0
11:11:18.082	35:23:8.26	1.7 ± 0.2		1.1 ±0.1	-0.5
11:24:03.341	-07:47:01.13	2.1 ± 0.1	3.7±0.6	1.2 ±0.1	-0.5
11:39:17.604	09:57:45.03	2 ± 0.1	±	1.1 ±0.1	-0.7

11:39:14.889	17:08:37.41	6.2 ± 0.1	6.6±0.5	4.9 ±0.1	-0.2
11:41:52.959	10:18:15.75	2.1 ± 0.1	2.9±0.4	1.5 ±0.1	-0.2
11:43:02.141	19:38:31.29	8.5 ± 0.1	6.7±0.5	5.4 ±0.1	-0.5
11:44:32.113	20:06:23.67	2.8 ± 0.2	3.1±0.4	1.5 ±0.1	-0.6
11:45:58.38	29:19:57.58	2 ± 0.2	±	1.6 ±0.1	-0.2
11:48:27.531	12:43:38.39	6.2 ± 0.2	8.8±1	0.7 ±0.1	-1.2
11:52:30.543	20:37:31.62	1.8 ± 0.2		0.7 ±0.1	-0.9
11:52:42.608	20:37:52.89	4.5 ± 0.2	5.5±0.4	3.9 ±0.1	-0.1
12:01:44.901	20:19:41.84	2.4 ± 0.1		1.5 ±0.1	-0.6
12:01:52.231	08:29:45.18	2.4 ± 0.1	3.4±0.4	1.2 ±0.1	-0.7
12:02:29.57	00:12:44.64	2.5 ± 0.2		1.4 ±0.1	-0.5
12:03:21.111	04:13:41.29	2.3 ± 0.2		2.5 ±0.1	-0.1
12:05:29.34	20:14:48.23	3.1 ± 0.1	8.4±1.3	2.5 ±0.1	-0.2
12:09:09.831	31:34:10.19	2.5 ± 0.1	4±0.5	2.6 ±0.1	0
12:05:48.207	20:27:48.27	6.9 ± 0.1		2 ±0.1	0.4
12:13:09.305	32:35:47.07	1.7 ± 0.2	2.2±0.4	2 ±0.1	0.2
12:14:53.824	22:08:22.56	2 ± 0.1		2.7 ±0.1	0.3
12:18:08.114	06:08:22.23	6 ± 0.1		3.2 ±0.1	-0.6
12:19:52.969	08:56:15.35	1.8 ± 0.1		0.9 ±0.1	-0.7
12:25:46.309	45:17:24.25	3.3 ± 0.1	3.8±0.4	0.9 ±0.1	-0.5
12:26:3.665	08:15:18.97	5.1 ± 0.2	2.9±0.4	1.7 ±0.1	-1.1
12:32:56.778	11:23:24.64	2.3 ± 0.2		2.1 ±0.1	-0.8
12:35:41.168	26:31:22.78	1.9 ± 0.2		0.7 ±0.1	-1.3
12:38:48.796	31:59:5.63	4.2 ± 0.1	4.8±0.4	2 ±0.1	-1
12:50:08.706	33:09:33.34	3.1 ± 0.2	7.4±1.1	2.1 ±0.1	-0.5
12:50:52.959	34:09:24.54	3.3 ± 0.1	3.3±0.5	2.1 ±0.1	-0.5
12:53:59.118	26:26:38.68	2.4 ± 0.1	4.1±0.5	2.8 ±0.1	0.2
13:07:8.149	46:18:34.24	1.5 ± 0.1		2 ±0.1	0.2
13:11:34.032	44:55:59.05	3.3 ± 0.1		1.7 ±0.1	-1.0
13:12:25.858	28:32:15.74	4.9 ± 0.1	5.1±0.4	3.1 ±0.1	-0.6
13:19:40.071	27:42:21.79	3.2 ± 0.1	6±1.2	2.1 ±0.1	-0.5
13:23:59.882	30:55:56.94	2.5 ± 0.1	2.7±0.5	1.5 ±0.1	-0.7
13:23:45.004	31:33:56.68	3.7 ± 0.1	158.7±5.1	3.2 ±0.1	-0.1
13:24:28.234	04:46:29.54	2.3 ± 0.1		1.6 ±0.1	-0.4
*13:26:51.288	26:35:28.53	1.7 ± 0.1	2.2±0.4	0.7 ±0.1	-1.2
13:29:30.908	11:44:44.77	1.8 ± 0.1		7.4 ±0.1	0.5
13:32:43.365	18:10:34.78	2.7 ± 0.1	3.8±0.4	3.0 ±0.1	0.1
13:34:13.828	09:38:08.01	2.2 ± 0.1		1.2 ±0.1	-0.6
13:34:25.231	34:41:26.07	1.6 ± 0.1	3.6±0.5	3 ±0.1	0.8
13:37:28.941	38:58:13.82	3.2 ± 0.2		1.1 ±0.1	-0.5
13:39:26.009	15:12:46.45	1.9 ± 0.1		1.8 ±0.1	-0.0
13:46:22.224	-03:25:6.81	3.2 ± 0.2	5.5±0.5	2 ±0.1	-0.5

13:56:04.438	38:18:15.27	2.8 ± 0.1	4.8±0.5	1.6 ±0.1	-0.7
*14:00:31.163	-02:51:39.17	1.1 ± 0.2		0.6 ±0.1	-0.8
14:00:37.212	-02:51:28.47	2.9 ± 0.2	6.4±0.5	2.1 ±0.1	-0.5
* 14:02:55.708	09:25:14.54	4.2 ± 0.2	6.9±0.5	1.1 ±0.1	-1.6
14:05:28.328	30:46:2.02	7.8 ± 0.1	7.2±0.5	9 ±0.1	0.2
14:08:04.001	07:19:40.07	2.8 ± 0.2	3.6±0.4	1.5 ±0.1	-0.6
*14:14:20.854	07:30:58.06	1.6 ± 0.2	2.3±0.5	0.9 ±0.1	-0.4
*14:14:30.535	06:09:55.42	1.7 ± 0.2		<0.4	<-1.9
*14:30:52.286	06:02:09.66	1.2 ± 0.1		<0.4	<-1.4
14:36:23.708	35:54:19.16	6 ± 0.1	5.5 ±0.4	3.6 ±0.1	-0.7
15:34:53.723	23:28:16.48	5.1 ± 0.1	4.4±0.4	7.4 ±0.1	0.5
15:39:27.5	24:56:51.51	9.3 ± 0.1	20.1±1	5.7 ±0.1	-0.6
15:59:13.913	19:43:15.09	5.6 ± 0.1	11.3±0.5	1.8 ±0.1	-0.3
16:04:28.18	14:46:56.84	3.7 ± 0.1	2.6±0.5	5.2 ±0.1	0.3
16:29:33.664	21:47:12.34	3.8 ± 0.1	3.7±0.4	3.7 ±0.1	-0.8
22:40:17.262	08:33:57.07	2 ± 0.1	9.4±0.9	3.0 ±0.1	-0.1
23:35:01.071	04:53:51.38	3.1 ± 0.1	8.7±0.5	9.0 ±0.1	0.2
23:35:10.457	04:57:51	5.3 ± 0.1	9.8±0.5	1.5 ±0.1	-0.8

Tabel 20: Table of sources studied in this work, which originally appeared in Ofek [2017], along with calculated peak fluxes and spectral indices. The starred sources are the ones we discuss in more detail in Section 4.3. The 10 sources located off-center within a host galaxy are in the first section before the dividing line, and the second contains either sources located at the center of a nearby galaxy or which appear far from the galaxy.